Neurobiology of Disease

Miz1 Controls Schwann Cell Proliferation via H3K36^{me2} Demethylase Kdm8 to Prevent Peripheral Nerve Demyelination

David Fuhrmann,[1] Marco Mernberger,[2,3] Andrea Nist,[2] Thorsten Stiewe,[2,3] and Hans-Peter Elsässer[1]

[1]Department of Cytobiology and Cytopathobiology, [2]Genomics Core Facility, and [3]Institute of Molecular Oncology, Philipps University, 35043 Marburg, Germany

Schwann cell differentiation and myelination depends on chromatin remodeling, histone acetylation, and methylation, which all affect Schwann cell proliferation. We previously reported that the deletion of the POZ (POxvirus and Zinc finger) domain of the transcription factor Miz1 (Myc-interacting zinc finger protein; encoded by *Zbtb17*) in mouse Schwann cells (*Miz1ΔPOZ*) causes a neuropathy at 90 d after birth [postnatal day (P) 90], with a subsequent spontaneous regeneration. Here we show that RNA sequencing from *Miz1ΔPOZ* and control animals at P30 revealed a set of upregulated genes with a strong correlation to cell-cycle regulation. Consistently, a subset of Schwann cells did not exit the cell cycle as observed in control animals and the growth fraction increased over time. From the RNAseq gene list, two direct Miz1 target genes were identified, one of which encodes the histone H3K36^{me2} demethylase Kdm8. We show that the expression of *Kdm8* is repressed by Miz1 and that its release in *Miz1ΔPOZ* cells induces a decrease of H3K36^{me2}, especially in deregulated cell-cycle-related genes. The linkage between elevated *Kdm8* expression, hypomethylation of H3K36 at cell-cycle-relevant genes, and the subsequent re-entering of adult Schwann cells into the cell cycle suggests that the release of *Kdm8* repression in the absence of a functional Miz1 is a central issue in the development of the *Miz1ΔPOZ* phenotype.

Key words: **histone demethylation; Kdm8; Miz1; peripheral neuropathy; proliferation; Schwann cell**

Significance Statement

The deletion of the Miz1 (Myc-interacting zinc finger protein 1) POZ (POxvirus and Zinc finger) domain in Schwann cells causes a neuropathy. Here we report sustained Schwann cell proliferation caused by an increased expression of the direct Miz1 target gene *Kdm8*, encoding a H3K36me2 demethylase. Hence, the demethylation of H3K36 is linked to the pathogenesis of a neuropathy.

Introduction

The zinc finger transcription factor Miz1 (Myc-interacting zinc finger protein 1; Zbtb17) was originally identified as a binding partner of the proto-oncogene Myc by a yeast two-hybrid approach (Peukert et al., 1997). Miz1 activity depends on a tetramerization mediated by the N-terminal BTB/POZ (Broad-Complex, Tramtrack, and Bric à brac/POx virus and Zinc finger) domain. Miz1 preferentially binds at the initiation region of a gene, using a consensus binding sequence that has recently been published (Wolf et al., 2013). Miz1 can recruit different cofactors that can either enhance its transactivation activity or function as corepressors in a cell-type-dependent and context-dependent manner (Herkert and Eilers, 2010). In neuronal progenitor cells from embryonic day (E) 13.5 brain (Wolf et al., 2013) and in the mammary gland epithelial cell line MDA-MB231 (Sanz-Moreno et al., 2014), 140–261 Miz1 binding sites were identified by chromatin immunoprecipitation (ChIP) analysis, illustrating the complexity of Miz1 regulatory networks.

The constitutive deletion of Miz1 is lethal at at day 7.5 of the embryonic development (Adhikary et al., 2003). Alternatively, the conditional deletion of the Miz1 POZ domain has been used in keratinocytes (Gebhardt et al., 2007; Hönnemann et al., 2012), hematopoetic precursor cells (Kosan et al., 2010; Möröy et al., 2011), mammary gland epithelial cells (Sanz-Moreno et al., 2014), and neuronal cells (Wolf et al., 2013) to investigate Miz1 gene regulatory functions. Recently, the deletion of the Miz1 POZ domain in Schwann cells, the glial cells of the peripheral nervous tissue, has been described (Fuhrmann and Elsässer, 2015; Sanz-Moreno et al., 2015). In this model, a diplegia of the hind limbs and an attenuated strength of the forelimbs are observed. This late-onset neuropathy is characterized by massive demyelination

Received March 28, 2017; revised Nov. 15, 2017; accepted Nov. 17, 2017.

Author contributions: H.-P.E. designed research; D.F. and A.N. performed research; T.S. contributed unpublished reagents/analytic tools; D.F., M.M., and H.-P.E. analyzed data; D.F. and H.-P.E. wrote the paper.

This work was supported by the Deutsche Forschungsgemeinschaft with the Grant EL-125/6-1. We thank Waltraud Ackermann, Julia Kirch, Uschi Lehr, and Tim Seiler for their excellent technical assistance. We thank Alexander Brehm, Bastian Stielow, and Elmar Wolf for helpful discussions. We thank Joseph Braymer for critically reading the manuscript.

The authors declare no competing financial interests.

Correspondence should be addressed to Dr. Hans-Peter Elsässer, Philipps University Marburg, Department of Cytobiology and Cytopathobiology, Robert-Koch Str. 6, 35033 Marburg, Germany. E-mail: elsaesse@mailer.uni-marburg.de.

DOI:10.1523/JNEUROSCI.0843-17.2017

 0270-6474/18/380858-20$15.00/0

Table 1. List of antibodies used

Antigens	Clonality	Host	Catalog #	Company	Immunohistochemistry	Western blotting	ChIP
GAPDH	Mono	Mouse	5G4-6C5	HyTest	—	1:2000	—
Histon H3	Poly	Rabbit	ab1791	Abcam	—	1:2000	—
H3K4me3	Mono	Rabbit	04-745	Millipore	—	1:2000	—
H3K9me3	Poly	Rabbit	ab8898	Abcam	—	1:2000	—
H3K36me2	Poly	Rabbit	C15310127	Diagenode	1:250*	1:2000	2 μg
JUN	Mono	Rabbit	9165	Cell Signal Technology	—	1:500	—
Ki67	Mono	Rat	M7249	Dako	1:200*	—	—
Miz1	Mono	Mouse	[a]	—	—	1:400	—
Miz1	Poly	Rabbit	sc-22837	Santa Cruz Biotechnology	—	—	3 μg
MPZ	Poly	Rabbit	ab31851	Abcam	—	1:1000	—
Myc-TAG	Poly	Rabbit	2272	Cell Signal Technology	—	1:1000	—
SOX10	Poly	Rabbit	SI058R06	DCS[b]	undiluted*	—	—
α-mouse HRP	Poly	Goat	172-1011	Bio-Rad	—	1:7500	—
α-rabbit HRP	Poly	Goat	172-1019	Bio-Rad	—	1:7500	—
α-rabbit A488	Poly	Goat	A-11008	Invitrogen	1:400	—	—
α-rabbit A546	Poly	Goat	A-11010	Invitrogen	1:400	—	—
α-rat A633	Poly	Goat	A-21094	Invitrogen	1:400	—	—

*Antigen retrieval was performed using 10 mM Tris, pH 9, and 1 mM EDTA in a steam cooker for 20 min.

[a]Gift from Martin Eilers, University of Würzburg.

[b]Dr. Christian Sartori GmbH & Co. KG.

and the degradation of myelin is accompanied by a high expression of genes indicative for reprogramming of mature Schwann cells to repair Schwann cells (Jessen and Mirsky, 2005, 2016). These genes include *Egr1*, *Jun*, and *Sox2* (Sanz-Moreno et al., 2015). In contrast, the expression of structural genes, such as *myelin protein zero* (*Mpz*), *myelin basic protein* (*Mbp*), or *periaxin* (*Prx*), is reduced (Sanz-Moreno et al., 2015). Interestingly, the obvious clinical traits disappear spontaneously between P120 and P150 and this acute episode does not recur, not even in animals >1 year old.

Here, we traced back the gene regulatory changes from P90 to P30, when the postnatal development is completed, to identify the initial mechanisms causing the observed neuropathy. Subsequently, we revealed an early upregulated gene set implicated in cell-division processes and increased Schwann cell proliferation in *Miz1ΔPOZ* animals already at P30, long before first ultrastructural changes occur. Furthermore, we were able to prove direct binding of Miz1 to the core promoter of early deregulated genes. One of these genes encodes the histone 3 (H3) demethylase Kdm8 (Jmjd5), which is involved in the regulation of the cell cycle (Hsia et al., 2010; Ishimura et al., 2012). We provide evidence that increased *Kdm8* expression supports Schwann cell proliferation via H3K36 demethylation. Last, we propose a model in which the deletion of the Miz1 POZ domain releases the transcriptional repression of *Kdm8* by Miz1, thereby compromising the complete arrest of Schwann cells in G0 and causing a major issue in the *Miz1ΔPOZ* neuropathy pathogenesis.

Materials and Methods

Animals

Miz1$^{lox/lox}$ mice were crossed with the desert hedgehog (*Dhh*)-*Cre* driver line [C57BL6-Tg(Dhh-cre)1Mejr] to achieve conditional ablation in Schwann cells of *Miz1* exons 3 and 4, which encode the POZ domain (Sanz-Moreno et al., 2015). Mice had a mixed C57BL6 and 129S2/SvHsd genetic background. Here, animals that were *Dhh-Cre*$^{+}$;*Miz1*$^{flox/flox}$ are designated *MizΔPOZ*. Genotyping was performed by standard PCR, using the REDExtract-N-Amp Tissue PCR Kit (XNATR; Sigma-Aldrich) and appropriate primers for *Cre* (GAACGCACTGATTTCGACCA; AACCAGCGTTTTCGTTCTGC) and for *Miz1* (GTATTCTGCTGTGG GGCTATC; GGCTGTGCTGGGGGAAATC; GGCAGTTACAGG CTC AGGTG). Research with mice was conducted according to the German Animal Protection Law (Tierschutzgesetz). The application for the experiments was reviewed and approved by the responsible local authorities (Regierungspraesidium Giessen, reference numbers V54-19c20 15h01-MR20/10 no. 14/2014 and V54-19c20 15h01-MR20/10 G58/2016).

Immunohistochemistry

Freshly dissected sciatic-nerve or small-intestine tissue was fixed in 3.7% formaldehyde overnight at 4°C. Tissue was dehydrated and embedded in paraffin and sections were stained following standard procedures. Briefly, sections were incubated overnight at 4°C with primary antibodies, and subsequently for 1 h at room temperature (RT) with fluorophore-conjugated secondary antibodies (Table 1). Cell nuclei were counterstained with Hoechst 34580 (Invitrogen, H21486). The TUNEL assay was performed following manufacturer's instructions (DeadEnd Fluorometric TUNEL System, Promega).

Five-ethynyl-2′-deoxyuridine injection and labeling

Mice were intraperitoneally injected once or seven times every 2 h with 100 μl of 2 μg/μl 5-ethynyl-2′-deoxyuridine (EdU; Roth, #7845.3) in PBS. Either 1 h after the single injection or 2 h after the last consecutive injection, mice were killed and sciatic nerves and a piece of the small intestine were dissected. Tissue was further processed as described above. EdU was detected by incubating the sections for 30 min in the dark with a freshly prepared solution of 2 mM $CuSO_4$, 20 μM 6-carboxyfluorescein azide (Baseclick, #BCFA-001), 100 mM ascorbic acid, and 100 mM Tris, pH 8.5. After three washes with TBS containing 0.5% Triton X-100, tissue sections were further subjected to immunohistochemical stainings as described above.

Image analysis

EdU/SOX10 quantification. To quantify proliferating cells and determine the proportion of proliferating Schwann cells, longitudinal sciatic-nerve sections immunostained with SOX10, counterstained with Hoechst 34580, and labeled with EdU were acquired on a BX61 Olympus microscope equipped with a F-View digital camera (Soft Imaging System). ImageJ analysis software was used to quantify the amount of SOX10-positive or Hoechst-labeled nuclei. Each channel was converted into a binary image, overlapping nuclei were discriminated using the watershed function, and nuclei were counted excluding signals with <60 or >1000 pixels. EdU-positive nuclei were counted manually and identified for costaining or not with SOX10.

TUNEL quantification. TUNEL-positive cells were counted manually and nuclei stained with Hoechst were quantified as described above.

Ki67/SOX10 quantification. Pictures of longitudinal sciatic-nerve sections double-immunostained with SOX10 and Ki67 were taken with a Leica DM IRE2/SP2 confocal scanning microscope with a 40× objective (HCX PL APO CS 40×/1.25–0.75 oil). Ki67-positive and SOX10-positive nuclei were counted manually using the Leica LAS AF Lite software (Leica).

EdU/H3K36me2 quantification. Longitudinal sciatic-nerve sections were obtained from four 30-d-old mice of each genotype that were injected seven times every 2 h with EdU. Sections were immunostained for H3K36me2, counterstained with Hoechst 34580, and labeled with EdU. Image-acquisition settings were the same for all samples, using a Leica DM IRE2/SP2 confocal scanning microscope with a 40× oil objective. Summed mean pixel intensity per area of all Hoechst-stained or H3K36me2-labeled nuclei was calculated using ImageJ analysis software. Staining intensity is presented as the ratio of H3K36me2 versus Hoechst 34580 staining intensity, to prevent bias from different nuclei numbers or sizes between different samples. The same ratio was determined manually for each EdU-labeled nuclei, using the intensity quantification tool of the LAS AF Lite software. Researchers taking the pictures had no knowledge of the genotypes of the samples.

Nerve-diameter quantification. Contralateral sciatic-nerve pairs were dissected and each nerve was cut in three pieces of similar sizes. The mean nerve diameter for each animal was determined with ImageJ measuring each of the six pieces together with a micrometer scale using an Olympus SZ61 stereo microscope.

Transmission electron microscopy

Sciatic-nerve fragments were fixed in a mixture of 2.5% glutaraldehyde, 2.5% paraformaldehyde, and 0.05% picric acid in 67 mM cacodylate buffer, pH 7.4, according to techniques described by Ito and Karnovsky (1968). Postfixation was performed in 1% osmium tetroxide and samples were embedded in Epon according to standard procedures. Thin sections were contrasted with lead citrate and uranyl acetate, and were examined with a Zeiss EM 109S electron microscope.

Cell culture and transient transfection

mSC80 cells were cultivated in DMEM (Biochrom, FG0415) containing 1 g/L glucose and was supplemented with 10% FBS (Biochrom, S0615), 1% stable glutamine (GE Healthcare, M11-006), and 1% gentamicin (PAA Laboratories, P11-004). RNAiMAX (Thermo Fisher Scientific, #13778075) and Opti-MEM (#31985062) were applied for siRNA transfections following the manufacturers' protocols. A combination of siRNA against murine *Zbtb17* (ON-TARGETplusSMARTpool, L-046195-01) and an off-target control (D-001630-01) were obtained from GE Dharmacon.

Plasmid constructs for the overexpression of human Myc-tagged *Kdm8* or the *Kdm8H321A* mutant were generously provided by Jimin Shao and Jing Shen (Huang et al., 2015). A plasmid carrying the full-length human *ZBTB17* cDNA was a generous gift from Martin Eilers (Staller et al., 2001). Target and empty control vectors were transiently transfected using Lipofectamine 2000 (Thermo Fisher Scientific, #11668027) according to the manufacturer's instructions or the calcium phosphate method (Jordan et al., 1996). Briefly, 5000–10,000 cells from the exponential growth phase were seeded per cm^2 into 12-well or 60 mm plates 24 h before transfection. One volume of 40 μg/ml DNA in 250 mM $CaCl_2$ was added dropwise to one volume of 2 × HBS buffer (280 mM NaCl, 1.5 mM Na_2HPO_4, 50 mM HEPES, pH 7.05) by vortexing. For each 12-well plate, 100 μl was added to the media. For each 60 mm plate, 500 μl was added. After 24 h, cells were washed with PBS and fresh media containing 5% FBS was added.

Cell growth-rate analysis

For determination of cell numbers, cells were seeded in 12-well plates and transiently transfected with indicated plasmids as outlined above. Protein quantity was measured via amido black staining (Palombella et al., 1988). Cells were washed three times with PBS and subsequently fixed for 15 min at RT with 37% formaldehyde 1:10 diluted in 0.1 M sodium acetate containing 9% acetic acid. Cells were washed with distilled water and stained for 30 min at RT with amido black solution (Serva, 12310.01). Finally, cells were washed thoroughly with distilled water and, finally, the amido black dye could be eluted using 1 ml of 50 mM NaOH. Four independent wells were analyzed for each experimental condition. Three times 200 μl of each well were transferred to a 96-well plate and absorbance was determined in triplicates at 620 nm in an Infinite200 microplate reader (Tecan). A standard curve was generated out of six known cell dilutions to estimate the corresponding cell numbers.

Quantitative reverse transcription PCR

Dissected sciatic-nerve pairs of indicated ages were homogenized in TRI Reagent (Sigma-Aldrich, T9424). RNA was extracted, Treated with DNase (Macherey-Nagel, #740963), and purified using the NucleoSpin RNA Clean-up kit (Macherey-Nagel, #740948), according to the manufacturers' instructions. RNA from cell-culture samples was extracted, treated with DNase, and isolated using the NucleoSpin RNA kit (Macherey-Nagel, #740955). cDNA was synthesized with the RevertAid first strand cDNA synthesis kit (Thermo Fisher Scientific, #K1622) using random hexamer primers and 0.1 μg of total RNA from sciatic nerves or 1 μg from cell-culture samples in 20 μl reactions. Real-time PCR was performed on a Mx3005P quantitative PCR system (Stratagene) in triplicate. Twenty-five microliter reactions including 2.5 μl of fivefold diluted cDNA, 12.5 μl of SYBR Green PCR master mix (Thermo Fisher Scientific, #AB1158), and each primer at 200 nM were set up. The primers used, purchased from Metabion, are depicted in Table 2. PCR amplification conditions were as follows: 95°C/15 min; 45 cycles of 95°C/30 s, 60°C/30 s, and 72°C/30 s. Gene expression was first normalized to *Gapdh*, then all samples were compared with a control animal by the $\Delta\Delta Ct$ method (Livak and Schmittgen, 2001). No template controls were included for each primer pair and product specificity was confirmed by dissociation curve analysis.

RNA sequencing and transcriptome analysis

RNA from sciatic nerves of 30-d-old animals was isolated and purified as described above for quantitative reverse transcription PCR (qRT-PCR). Integrity of total RNA was assessed on the Bio-Rad Experion. Sequencing libraries were prepared with the TruSeq Stranded mRNA Kit (Illumina). On-board cluster generation using the TruSeq Rapid SR Cluster Kit-HS (Illumina) and single-read 50 nt sequencing was performed on a HiSeq Rapid SR Flow Cell (Illumina) on the Illumina 1500 platform.

Illumina output bcl-files were converted and demultiplexed using the Illumina bcl2fastq script, version 1.8.3. Sequenced reads were aligned to the *Mus musculus* Ensembl reference genome (release 74, GRCm38) using STAR (Spliced Transcripts Alignment to a Reference; Dobin et al., 2013).

Gene read counts were established as read counts within merged exons of protein-coding transcripts (for genes with annotated protein gene product) or within merged exons of all transcripts (for noncoding genes). Fragments per kilobase per million (FPKM) were based on the total raw read count per gene and length of merged exons. Differential expression was assessed for genes with a minimum FPKM value of 0.3 in ≥1 sample using DEseq2 (Love et al., 2014). Thus, derived p values were subjected to Benjamini–Hochberg adjustment to correct for multiple hypothesis testing. To also include smaller differences in expression change between conditions, we considered genes as differentially expressed if a fold change of ≥2 or 1.5 was observed (indicated in the text) with an adjusted p value of <0.05.

RNAseq data has been deposited in the EBI ArrayExpress archive (http://www.ebi.ac.uk/arrayexpress/) and is accessible via the accession numbers E-MTAB-5600.

ChIP

mSC80 cells were cross-linked with 1% formaldehyde for 10 min at RT, subsequently quenched for 10 min with 125 mM glycine, and washed three times with PBS. Cells were successively lysed in LB1 (5 mM PIPES, 85 mM KCl, 0.5% NP40, pH 8) for 20 min and LB2 (10 mM Tris, 1 mM EDTA, 150 mM NaCl, 1% Sodium deoxycholate ($C_{24}H_{39}NaO_4$), 1% NP40, 0.1% SDS, pH 7.5), containing protease inhibitors (Roche, #04693116001), for 10 min. By using a Bioruptor (Diagenode) and applying 20 cycles (30 s on/90 s off) at high power, chromatin was sheared to an average size of 100–300 bp. Fragment size was checked on a 2% agarose gel. ChIP was performed with 3 μg of anti-Miz1 H190 antibody (Santa Cruz Biotechnology, #sc-22837) or a species-matched IgG control

Table 2. List of qRT-PCR primers used

Gene ID	Primer sequence (5′-3′)	Exon junction	Amplicon
Adgre1	fw: GGAGGACTTCTCCAAGCC rv: AGGCCTCTCAGACTTCTG	Exon 14/15	70 bp
Cdc20	fw: GCCCACCAAAAAGGAGCATC rv: ATTCTGAGGTTTGCCGCTGA	Exon 2/3	100 bp
Cdk1	fw: ACACACGAGGTAGTGACGCT rv: CAGATGTCAACCGGAGTGGA	Exon 5/6	83 bp
Cdk4	fw: GAGCGTAAGATCCCCTGCTTC rv: GGCTTTGTACACCGTCCCAT	Exon 1/2	94 bp
Cdk6	fw: ACCCACAGAAACCATAAAGGATA rv: GCGGTTTCAGATCACGATGC	Exon 3/4	94 bp
Cdkn1a	fw: TCCACAGCGATATCCAGACA rv: GGCACACTTTGCTCCTGTG	Exon 1/2	90 bp
Ccl2	fw: CATCCACGTGTTGGCTCA rv: GATCATCTTGCTGGTGAATGAGT	Exon 1/2	76 bp
Ccna2	fw: CAAGACTCGACGGGTTGCTC rv: TCCATGAAGGACCAGCAGTG	Exon 2/3	74 bp
Ccnb2	fw: CCGACGGTGTCCAGTGATTT rv: GCCGGATAGTCACATGGCTC	Exon 1/2	76 bp
Ccnd1	fw: CAAGTGTGACCCGGACTGC rv: TTGACTCCAGAAGGGCTTCAA	Exon 3/4	62 bp
Ccnd2	fw: CTGCGGAAAAGCTGTGCATT rv: CTGCGGAAAAGCTGTGCATT	Exon 2/3	72 bp
Ccne1	fw: GACACAGCTTCGGGTCTGAG rv: TGGTCCGTCGAGTCTCTCTC	Exon 1/2	71 bp
Cenpf	fw: ACAGCACAGTATGACCAGGC rv: AGCACTCTCTGCGTTCTGTC	Exon 7/8	105 bp
Ckap2	fw: GAGGAATCCCTTGCCGGTG rv: TGTTTTCTTTGTTCTCGGAAGGC	Exon 1/2	84 bp
E2F1	fw: GCAGATGGTGGGGCTGATATT rv: CCGTTTCACCTCCAACAAGC	Exon 1/2	97 bp
Fam64	fw: CCCCTGTTCCTCCACAGAAC rv: TGTCCAGCCTTTGAGACAGC	Exon 3/4	110 bp
Foxm1	fw: CTGTGAGGGTCAAAGCTTGC rv: GTCTTTTGAGAATCAGTGGCCG	Exon 1/2	94 bp
Iqgap3	fw: CTCGGACAGCCTATGAGCG rv: AGCCGGCAGAGGTACTGATA	Exon 1/2	85 bp
Itgam	fw: CCTTGTGGGTAAGCATAGCTAAAT rv: CAGCTCACACAAACAAGGAAATA	—	75 bp
Jun	fw: CCAGAAGATGGTGTGGTGTTT rv: CTGACCCTCTCCCCTTGC	—	63 bp
Kdm8	fw: AAAGTTGTCGCAGTCCTCCA rv: CGTCACACTTTGCCTTCTTGG	Exon 2/3	100 bp
Kif20a	fw: GTCCGAAAGGACCTGTTGTC rv: CTCCAGTAGAGCCTGCTTGT	Exon 2/3	72 bp
Kif2c	fw: AGTCCATGGAGTCGCTTCAC rv: GCGGGGTGAATTAAGCCATT	Exon 1/2	82 bp
Kif22	fw: GTGAGGTGGAGGACTTGGAAC rv: GCTCAAGAGATTCGCCTTCA	Exon 13/14	80 bp
Kif4	fw: GGCCTCCACAGCTATGAACT rv: ATGCAGCTTGGAACGAAAGC	Exon 5/6	112 bp
Mbp	fw: TGGCCACAGCAAGTACCAT rv: AGTCAAGGATGCCCGTGT	—	75 bp
Mki67	fw: GCTGTCCTCAAGACAATCATCA rv: GGCGTTATCCCAGGAGACT	Exon 7/8	71 bp
Mpz	fw: CCCTGGCCATTGTGGTTTAC rv: CCATTCACTGGACCAGAAGGAG	—	92 bp
Nsd1	fw: ATTCTCGGGGCCGTCCAATA rv: CTGTGCCTGCATCAACCTCA	Exon 1/2	95 bp
Nsd2	fw: GAGTACGTGTGTCAGCTGTG rv: CTTCGGGAAAGTCCAAGGCA	Exon 9/10	101 bp
Nsd3	fw: CGGTGTCTCTCCTGTGATCG rv: TCTCTCATCGAGCCTTCAGT	Exon 1/2	73 bp
Nrg1 (I)	fw: GGGAAGGGCAAGAAGAAGG rv: TTTCACACCGAAGCACGAGC	—	145 bp

(*Table continues*)

Table 2. Continued

Gene ID	Primer sequence (5′-3′)	Exon junction	Amplicon
Plk1	fw: GGTTTTCAATCGCTCCCAGC rv: AGGGGGTTCTCCACACCTTT	Exon 5/6	82 bp
Prc1	fw: CCAAACAGGAGAGGCAACTG rv: GACTTCTTGGGCGTCTGTCC	Exon 10/11	109 bp
Prx	fw: AGGAGCTCTGGAGGTGTCTGG rv: TCTTGAGTGATGGCCTTTTC	Exon 1/3	170 bp
Psrc1	fw: TCCCGGGAACTGGGAGATT rv: GGCTTAGACCTCGCTTCACA	Exon 1/2	65 bp
Setd	fw: CCCGACCCCTGAAGAAGAAG rv: CCCGACCCCTGAAGAAGAAG	Exon 1/2	87 bp
Setmar	fw: GGCCTAAACCTTTCCAGCTACT rv: CCGGGTGCTGTCTTACTCAG	Exon 1/2	107 bp
Sox2	fw: TCCAAAAACTAATCACAACAATCG rv: GAAGTGCAATTGGGATGAAAA	—	73 bp
Top2a	fw: CGAGAAGTGAAGGTTGCCCA rv: CCCACAAAATTCTGCGCCAA	Exon 19/20	113 bp
Tpx2	fw: ATAGGCGAGCCTTTTCAGGG rv: CAACTGCCTTCAACGGTGTG	Exon 4/5	82 bp
Zbtb17	fw: AGGCACACTGTCTGAGAAGAGA rv: TGGTTCAGCTGCTCCAAGA	Exon 2/3	96 bp
Znhit3	fw: GAAGCCGAAATACCGTTGCC rv: AGCTGCACTGCTCTTTGTGC	Exon 1/2	83 bp

using the One Day ChIP kit (Diagenode, #C01010081) following the manufacturer's instructions.

Dissected sciatic nerves from 10 mice were homogenized in liquid nitrogen and directly cross-linked with 1% formaldehyde for 16 min at RT. Quenching, washing, lysis and chromatin shearing of the *in vivo* samples were performed as described for mSC80 cells with the exception that the Bioruptor was used for 20 min (30 s on/30 s off) at medium power and 3× for 20 min at high-power settings. Histone methylation ChIP was also performed as described for mSC80 cells, using 2 μg of specific H3K36^{me2} antibody (Diagenode, C15310127) or rabbit IgG control. Anti-Miz1 immunoprecipitation was conducted on 100 μl of sheared chromatin with 3 μg of H190 antibody (Santa Cruz Biotechnology, #sc-22837) or rabbit IgG control using the One Day ChIP kit. In derogation from the manufacturer's instructions were followed except that DNA was eluted from the antibody-binding beads with 100 mM $NaHCO_3$ containing 1% SDS and was further purified as follows: All samples were treated with 1 μl of RNase (10 μg/μl) for 1 h at 37°C. Subsequently, samples were incubated at 65°C overnight for cross-linking reversal. After treatment with 3 μl of proteinase K (10 μg/μl) for 2 h at 45°C, DNA was purified on QIAquick columns (Qiagen, #28104) following the manufacturer's protocol. DNA of three H190-treated or IgG-treated immunoprecipitation samples was pooled on one column to increase the amount of DNA. Two microliters of purified ChIP DNA were subjected to qPCR, described above, using primers summarized in Table 3 (H3K36^{me2}) and Table 4 (H190). Results are presented as the percentage of input.

Western blotting

Snap-frozen sciatic-nerve pairs or mSC80 cells were homogenized in ice-cold RIPA buffer (150 mM sodium chloride, 1% Triton X-100, 0.5% Sodium deoxycholate, 0.1% SDS, and 50 mM Tris, pH 8) containing protease inhibitors (Roche, #04693116001) and benzonase (Novagen, #70664-3). Homogenates were maintained at constant agitation for 2 h at 4°C and then centrifuged at 13,000 × *g* for 20 min at 4°C to remove cellular debris. Protein concentrations were determined using a BCA assay (Sigma-Aldrich, B9643). Twenty micrograms of the samples were resolved by SDS-PAGE on 8–20% gradient gels, transferred to nitrocellulose membranes, and incubated with antibodies listed in Table 1. Western blots were quantified by densitometry using LabImage 1D software (Kapelan).

Statistical analysis

All data are expressed as mean ± SEM. unless indicated otherwise. Statistical differences of one continuous variable between two groups were

Table 3. List of H3K36me2 ChIP-qPCR primers used

Gene ID	Primer sequence (5′-3′)	Location	Amplicon
Psrc1 TSS	fw: GCAAGGAAACCCAGTCTCAGA rv: GGGGAGAACTGTCGAACCAA	TSS	78 bp
Psrc1 exon	fw: ATCCCAGCACTCTAGAGGCA rv: GGCTGTCCTGGAACTCACTC	Exon	82 bp
Iqgap3 TSS	fw: TCGGACAGCCTGTGAGTG rv: GAAAACCAAGCCCCGCCA	TSS	70 bp
Iqgap3 exon	fw: TCTTGTCCTGAGCCAGCTTG rv: AGAAATGGTGATCGGGCTGG	Exon	84 bp
Ckap2 TSS	fw: CAGCATTTGACAGGTGCAGT rv: TCTTCAGACACAGCCCAGAG	TSS	60 bp
Ckap2 exon	fw: TAAACCTGTGAGCACTGCGT rv: GTGGGAACTACTGTGGAGGC	Exon	73 bp
Top2a TSS	fw: GTCTCTCAGAGCACATGGACC rv: GGCGGGAGAATCTTCAAAATGG	TSS	93 bp
Top2a exon	fw: CCCAGTACCAAGATGCTGCT rv: CCGCAGAAAGGGTGTCTGAT	Exon	71 bp

Exon: coding region at the 3′ end of the gene indicated.

determined using the two-tailed, unpaired Student's *t* test. Comparisons between multiple groups were analyzed using two-way ANOVA followed by Bonferroni's post-tests comparing each column with each other. Statistical differences were considered significant for $p < 0.05$ ($^{*}p < 0.05$, $^{**}p < 0.01$, $^{***}p < 0.001$). Statistical analysis was performed using GraphPad Prism (GraphPad Software). Statistical information in all figures represent results obtained by the two-tailed, unpaired Student's *t* test unless indicated otherwise.

Results

Time course of the *Miz1ΔPOZ* neuropathy reveals initial transcriptional changes that track to the end of postnatal development

In a previous study, we reported that the deletion of the Miz1 POZ domain in Schwann cells (*Miz1ΔPOZ*) causes a paralysis of the hind limbs in adult P90 *Miz1ΔPOZ* mice. Strikingly, at P30, *Miz1ΔPOZ* mice exhibited ordinary developed peripheral nerves, indistinguishable ultrastructurally from control animals, and did not show any clinical symptoms of moving disabilities (Sanz-Moreno et al., 2015). In the present study, we hypothesized that initial gene-regulatory changes, due to the ablation of the transcription factor Miz1, must occur eventually between P30 and P90. To identify the age of first pathological gene-expression alterations in *Miz1ΔPOZ* nerves, we chose here a predefined literature-based gene set implicated in myelination (*Mpz*, *Prx*, *Mbp*), dedifferentiation (*Jun*, *Sox2*, *Nrg1(I)*), or macrophage attraction (*Ccl2*) and invasion (*Adgre1*, *Itgam*).

Using qRT-PCR, we followed up the time course of this gene-expression pattern measuring gene expression at P30, P45, P60, P75, and P90. As already known from our previous study, the expression of the myelin protein genes *Mbp*, *Mpz*, and *Prx* in *Miz1ΔPOZ* mice was decreased at P90, thereby reflecting the observed demyelination (Fig. 1*A*). While *Mbp* expression was already diminished at P75, *Mpz* and *Prx* were still unaltered at this time point. None of the three genes was differently expressed in *Miz1ΔPOZ* versus control nerve tissue at P30–P60.

In peripheral nerves, injuries are accompanied by the reprogramming of mature Schwann cells into repair cells, in a process referred to as dedifferentiation (Jessen and Mirsky, 2016). Expression of dedifferentiation markers, such as *Jun*, *Sox2*, and *Nrg1(I)*, became elevated in *Miz1ΔPOZ* mice at an even earlier stage as the myelination markers and progressively increased until P90 (Fig. 1*B*). The expression of *Jun*, which is the master regulator for the Schwann cell repair program, and *Sox2* are earliest upregulated at P60. In contrast, *Nrg1(I)* expression was already increased at P30 in *Miz1ΔPOZ* animals, but its expression escalated at P60 and was also progressive until P90. The high-fold change for *Nrg1(I)* (≤150-fold) indicates that this gene is expressed, if at all, only at a very low level in control animals. Simultaneously to the dedifferentiation genes, the expression of macrophage marker genes, such as *Adgre* (encoding F4/80) and *Itgam* (encoding CD11b/MAC1), increased, indicating that a macrophage invasion takes place in parallel to the demyelination, most probably to support myelin clearance (Fig. 1*C*). This observation is supported by the expression of a major monocyte/macrophage chemoattractant cytokine *Ccl2* (encoding MCP1), which was significantly elevated in *Miz1ΔPOZ* nerve tissue already at P45 (Fig. 1*C*). The changes in the gene-expression pattern could be verified on the protein level, as shown, for example, for Jun and Mpz (Fig. 1*D*). Together, the upregulation of the dedifferentiation and macrophage marker gene-expression precedes the downregulation of myelin markers.

Finally, to assess whether the progressive transcriptional changes in *Miz1ΔPOZ* nerve tissue has any impact on the ultrastructure of the Schwann cells, we performed an electron microscopic analysis at P60 and at P75. We found myelin loops, autophagic myelin degradation, myelin clearance by macrophages, and hypomyelination (Fig. 2) all typically observed during the acute phase between P90 and P120 (Sanz-Moreno et al., 2015). While these features occurred only occasionally in *Miz1ΔPOZ* animals at P60, the phenotype was distinct at P75. Thus, the slight upregulation of *Nrg1(I)* (P30) and *Ccl2* (P45) precedes the onset of enhanced expression of dedifferentiation genes (P60), which was attended by morphological changes indicating dysmyelination and demyelination.

Identification of an early deregulated gene set is associated with cell division in *Miz1ΔPOZ* cells

For our further analysis, we chose P30 as a time when postnatal development is completed and the *Miz1ΔPOZ* phenotype has not yet emerged. Genes deregulated at this young age are promising candidates to be under direct transcriptional control of Miz1 and to cause the observed demyelinating neuropathy in *Miz1ΔPOZ* sciatic nerves. Consequently, to identify initial expression changes in *Miz1ΔPOZ* animals, we performed genome-wide transcriptome analysis using RNA sequencing (RNAseq) technology of P30 control and *Miz1ΔPOZ* nerve tissue.

As expected, transcriptome analysis revealed a concise number of twofold or almost twofold regulated genes and a highly significant Benjamini-Hochberg adjusted *p*-value of $<10^{-6}$ (Fig. 3*A*,*B*). Interestingly, two of these genes, namely *Znhit3* and *Kdm8*, were previously identified among 261 Miz1 target genes in an *in vitro* ChIPseq approach (Wolf et al., 2013). Because *Nrg1(I)* is not a known RefSeq gene, it is not on this gene list. Biological reliability of this list could further be validated by qRT-PCR with RNA samples from P30 sciatic nerves (Fig. 3*C*). Moreover, all upregulated genes from P30 were also upregulated at P90 but to a higher extent, indicating a progressive deregulation of the early identified genes (Fig. 3*D*). Using gene ontology (GO) analysis, we found that known functions of these genes were almost exclusively related to cell-cycle and cell-division processes (Fig. 3*E*).

To confirm this decisive GO result, we extended the gene list by lowering the threshold to a 1.5-fold expression change, revealing 117 upregulated and 40 downregulated genes, respectively, and GO analysis of the upregulated genes exhibited nearly the

Table 4. Identification of *Kdm8* and *Znhit3* as direct Miz1 target genes

Gene	Primer sequence	INR motif	MIZ1 motif	Amplicon	Fold enrichment
Tnfaip2	AGGCGTTGAGATGGAAGAGG CGTCACACAGTCAGCACCTA	−145	−144	−172 to −114	1.000 ± 0.046
Tnfaip2	GAACTCGTGGCTCCCTGT GGTCACTTTGCTGTTCCCAA	−1	−144	−34 to 36	0.995 ± 0.045
Crlf1	CGCCTTGTCAATTTCGGCTG CAGATTGGGGCTCGGGTC	−26	—	−33 to 54	1.375 ± 0.365
Psrc1	GCAAGGAAACCCAGTCTCAGA GGGGAGAACTGTCGAACCAA	−333	—	−333 to −255	1.105 ± 0.045
Klk8	TCACAAGTGGGCCAGAACTC GCAGAGCTCTAGATCCCCGA	−168 −141/155	318	249 to 338	1.045 ± 0.095
Hmmr	CGACGATCAGGAGCAGCC CACTAGATTCCTACCGCCGC	−131	—	−166 to −106	1.345 ± 0.065
Iqgap3	TCGGACAGCCTGTGAGTG GAAAACCAAGCCCCGCCA	280	150	111 to 180	0.805 ± 0,155
Ckap2	CAGCATTTGACAGGTGCAGT TCTTCAGACACAGCCCAGAG	−171	−239	−260 to −200	1.045 ± 0.025
Top2a	GTCTCTCAGAGCACATGGACC GGCGGGAGAATCTTCAAAATGG	−222	—	−254 to −161	1.075 ± 0.125
Kif20a	CACGCCTGAGAATTGGGATG GGACAGGCAGTGAGTATCGG	−130	—	−158 to −77	1.150 ± 0.010
Lipo1	ACCTGCATTCTTCACAACTTTGG ACATTGGCTCCTCAGTGACC	−219	—	−259 to −188	0.950 ± 0.110
Cenpf	GCACAGACCTCACCTTACCC GCGGGTCTGAATGAGGGTTA	−254	—	−316 to −244	0.930 ± 0.090
Tpx2	CTCTCTGATTGGTGCGTTCG CCGCGTCAGGACTCAACT	50	58	15 to 87	1.595 ± 0.375
Pbk	GCTATGTCTTTCTAGCCATCGC TTCGCACAGTCCTCCCAG	−71	—	−122 to −29	0.935 ± 0.015
Mki67	CTTCCCCAATCCTCTGTCGC AACGGCGGTTCAAATTCTGG	−188	—	−193 to −102	1.130 ± 0.090
Prc1	TAGGCGGTCTCTGTATCCCA GACAATTGGTTACCGCGTCC	−220/−212	−108	−126 to −27	1.183 ± 0.494
Kif4	TGTCACCACTTCCAACCTAGG ATGGGATAGTTAAGAGTTGGCAC	−89	—	−94 to −1	1.095 ± 0.105
Kif22	GAAGGAAAAGTCGGGCGAAA TGAGGTCCCTGCACTTTCAG	−233	—	−265 to 206	1.130 ± 0.086
Fam64	GAGGACCGATAAGAAGGCCC TCTAACTGGCCACACTCAGC	−493	—	−543 to −459	1.125 ± 0.095
Kif2c	ACTGGTGACGTTGTAGGGAG CGACTCTGCTAATACTGCGC	−235/−75	61	10 to 98	1.295 ± 0.275
Eda2r	CCTCCCTAGACCCAGCTTCA TGAGTCTGGCGGGTAAACAC	−179/−139 −108/−64	—	−184 to −99	0.940 ± 0.070
Nusap1	AAAACAAACCCCTCCCTCCC TGAGTGAGGCGAGGGTAGTT	−189/160	—	−234 to −141	1.070 ± 0.240
Nrg1(I)	GGACTTCCCCAAAACTTGTGG CTCGCATCTCCCGGCAG	—	−3	−63 to 27	1.309 ± 0.409
Kdm8	CGATCAGCCGAGTCAGAAGT CTTCGGCTGGCTTTATCACC	148	36	−14 to 48	158.5 ± 23.69
Znhit3	CGACACTCTACAGGTGAGGC TGGCAGTCAGAAGCAATGGA	−370	−108	−107 to −65	119.6 ± 13.76

The table documents the primers used for the ChIP analysis using the anti-Miz1 antibody H190, and the fold enrichment obtained. INR, Initiation region; Miz1 motif, Position of the Miz1 consensus binding region, if one were found by the MAST algorithm; Amplicon, amplified region. Numbers indicate the position in relation to the TSS.

same biological processes (data not shown). In contrast, the set of downregulated genes did not identify a coherent biological process in the GO analysis (data not shown). In line with this notion, we found that of the 35 genes associated with the biological process of cell division, 34 genes were upregulated (Fig. 4*A*). Strikingly, most of these genes were preferentially associated with the G2/M phase and this was evaluated by qRT-PCR for an exemplary subset (Fig. 4*B*). Notably, polo kinase (PLK) 1, which is transcriptionally controlled by the transcription factor forkhead box M1 (Foxm1), plays a pivotal role in G2/M progression of the cell cycle (Combes et al., 2017). For example, PLK1 promotes the assembly of the mitosis promoting factor composed of the cyclin-dependent kinase 1 (Cdk1) and cyclin B (Ccnb), replacing the early G2/M cyclin A (Ccna). PLK1 also participates in the activation of CDC20 (cell division cycle 20), the key activator of the anaphase promoting complex (Zitouni et al., 2014). In contrast, key players in the regulation of the G1/S phases in the cell cycle did not show significant expression differences between control and *Miz1ΔPOZ* nerve tissue (Fig. 4*C*).

RNAseq analysis clearly pointed toward an increased proliferation as an early response to the deletion of the Miz1 POZ domain in *Miz1ΔPOZ* sciatic nerves. This proliferation is associated with a changed expression pattern of genes involved in the regulation of the G2/M phases of the cell cycle.

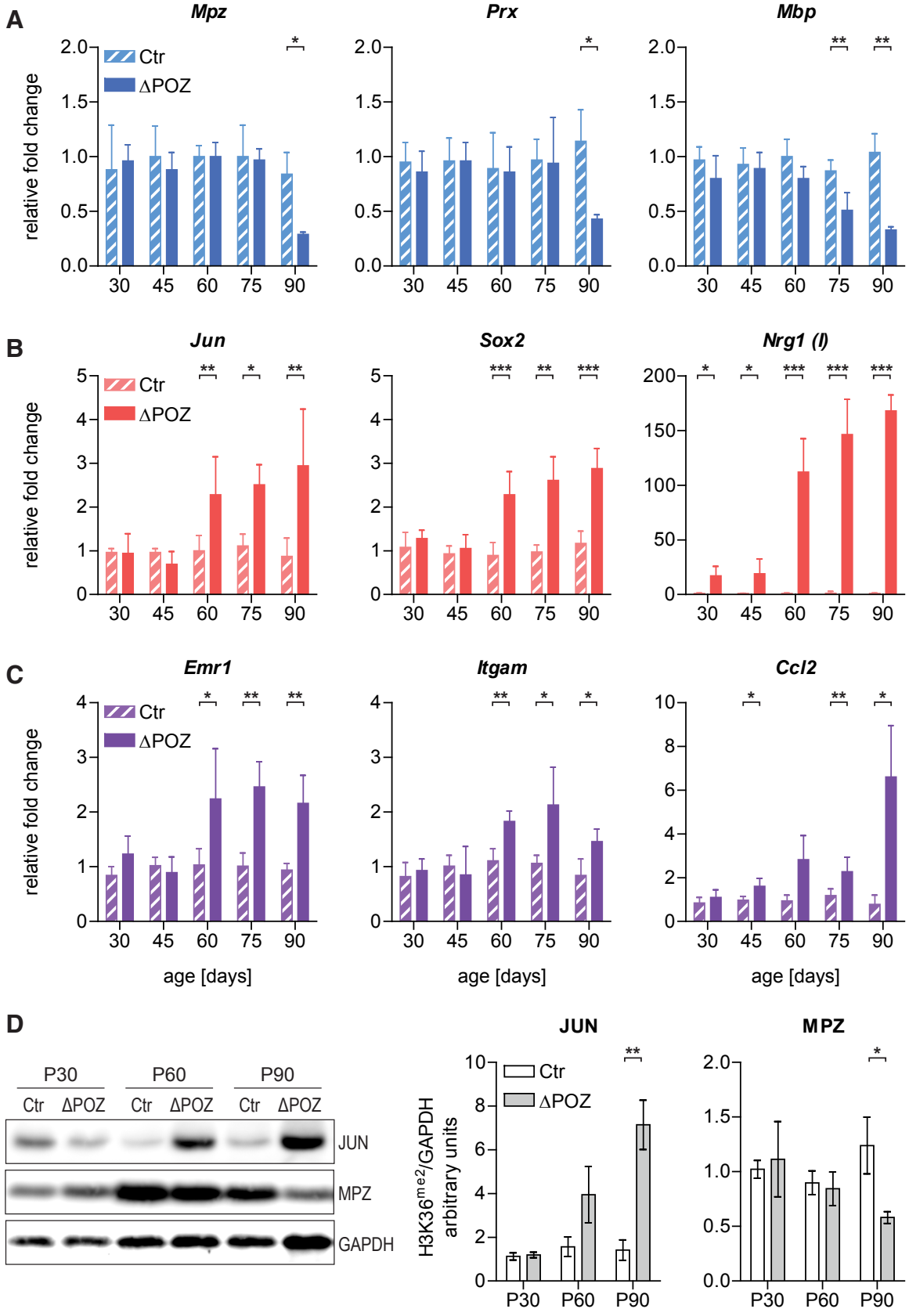

Figure 1. Time course analysis reveals initial transcriptional changes in *Miz1ΔPOZ* nerves. ***A–C***, Gene expression relative to *Gapdh* determined by qRT-PCR analysis of control (Ctr) and *Miz1ΔPOZ* sciatic-nerve samples at indicated ages for genes implicated in (***A***) myelination, (***B***) dedifferentiation, and (***C***) macrophage invasion or attraction. $n = 4$ animals per genotype and time point. ***D***, Western blot analysis of sciatic nerve homogenates from Ctr and *Miz1ΔPOZ* animals of indicated ages using antibodies against Jun, Mpz (P0), or Gapdh. Right, Signal intensity quantification of Jun or Mpz (P0) relative to *Gapdh*. $n = 3–4$ animals per genotype and time point. ***A–D***, Asterisks indicate the results of a two-tailed, unpaired Student's t-test (*$p < 0.05$, **$p < 0.01$, ***$p < 0.001$).

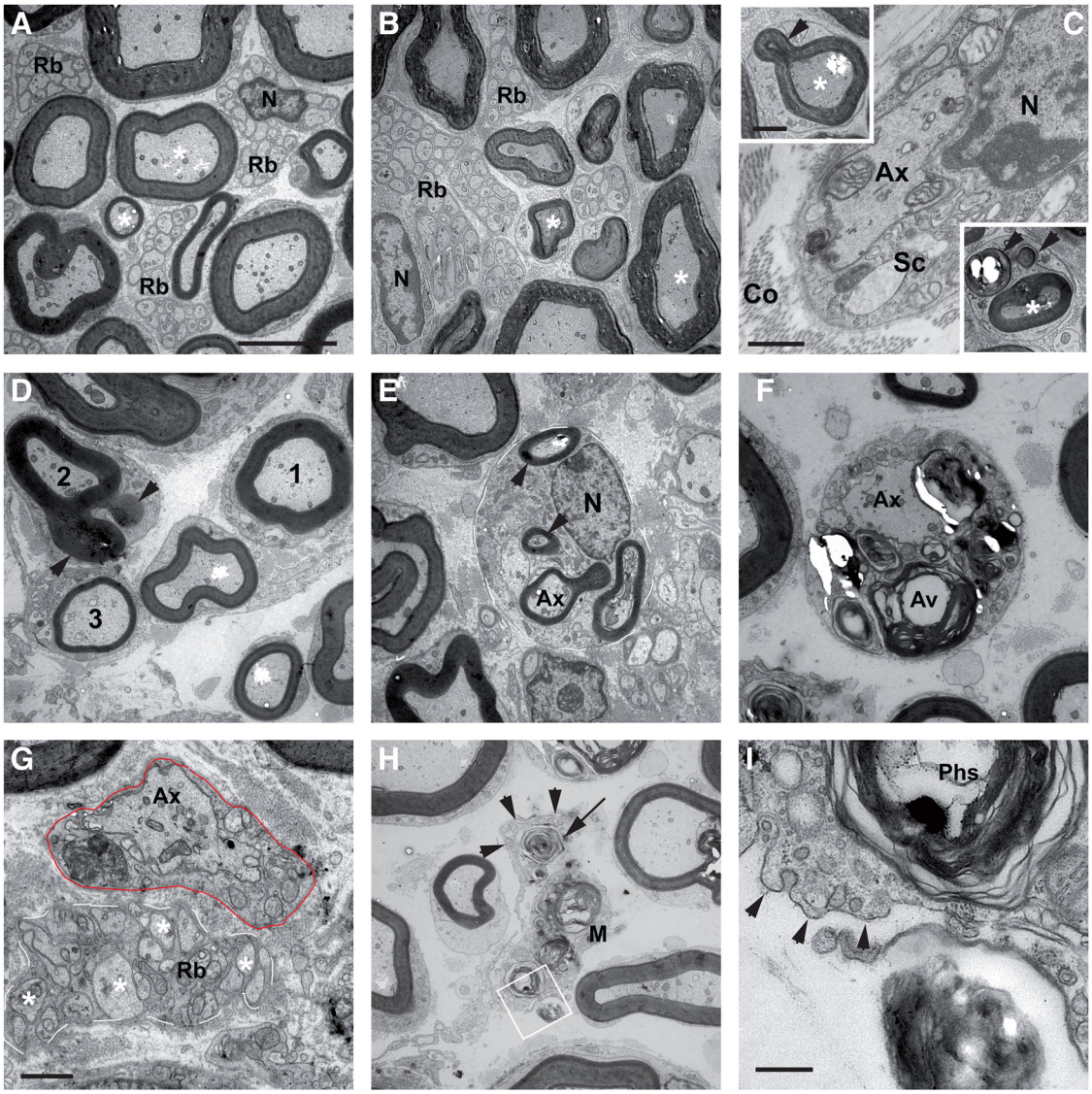

Figure 2. Ultrastructure of the sciatic nerve from P60 and P75 control and *Miz1ΔPOZ* animals reveal signs of demyelination and dysmyelination. ***A***, Nerve from a P75 control animal showing densely packed myelinated (*) axons and Remak bundles (Rb), which contain the unmyelinated axons. ***B***, Nerve from a P60 *Miz1ΔPOZ* animal, which appears to be similar to nerves from control animals. ***C***, However, at P60 *Miz1ΔPOZ* mice exhibit occasionally demyelinated axons and myelin loops (arrowheads in the insets), which indicate demyelination. ***D–G***, In P75 *Miz1ΔPOZ* animals, demyelination occurred extensively, with different grades of myelin loops (***D***, arrowheads at axon 2, ***E***) and autophagic degradation of myelin by Schwann cells (***F***), resulting in demyelinated (***G***) or hypomyelinated (***D***, compare 3 with the normal-appearing axon 1) axons. Line in ***E*** marks a Schwann cell with extensive myelin loops (arrowheads). Note that in ***G*** the different size of the unmyelinated axons in the Remak bundle (white line) compared with the demyelinated axon (Ax) in the adjacent Schwann cell (red line). ***H***, In the extracellular space, myelin debris (arrow) is phagocytosed by macrophages (M and arrowheads). ***I***, Higher magnification of area shown in white rectangle in ***H***. Note that this cell has no basement membrane and is thus not a Schwann cell. N, Nucleus; Co, collagen fibers; Sc, Schwann cell.

Deletion of the Miz1 POZ domain keeps Schwann cells cycling

The strong correlation of the upregulated genes with cell division prompted us to further analyze the proliferation of Schwann cells. As shown previously (Sanz-Moreno et al., 2015), at P90 Schwann cells as well as macrophages were positive for Ki67 in *Miz1ΔPOZ* mice. To elaborate the role of proliferation in *Miz1ΔPOZ* Schwann cells, we obtained the labeling index of cells that incorporated the thymidine analog EdU and were simultaneously positive for the Schwann cell marker Sox10 (Fig. 5*A*).

At P30, when the postnatal development of the peripheral nerve system in mice is completed, there was already a significant difference of EdU-positive cells between control and *Miz1ΔPOZ* animals (Fig. 5*B*). Moreover, while essentially no EdU-positive Schwann cells were detected in control animals at P60 and P90, the EdU-labeling index of *Miz1ΔPOZ* Schwann cells increased over time (Fig. 5*B*). This was confirmed by the Ki67-labeling index showing the same time course (Fig. 5*C*). As expected, the total amount of Ki67-positive Schwann cells is higher than that of EdU-positive Schwann cells, since EdU is incorporated only during the S phase of the cell cycle, while Ki67 is expressed during almost the whole cell cycle. Schwann cell proliferation was still detected at P400 in *Miz1ΔPOZ* animals, but the EdU-labeling and the Ki67-labeling index was, compared with P90, reduced to the same level as seen at P30 (Fig. 5*B*,*C*). To estimate the percentage of all Schwann cells being in the cell cycle at a given time after birth, we measured the growth fraction as the EdU-labeling index after seven repetitive EdU injections over 16 h (Nowakowski et al., 1989). Effective EdU injection was verified in sections of small intestine for each animal (data not shown). Remarkably,

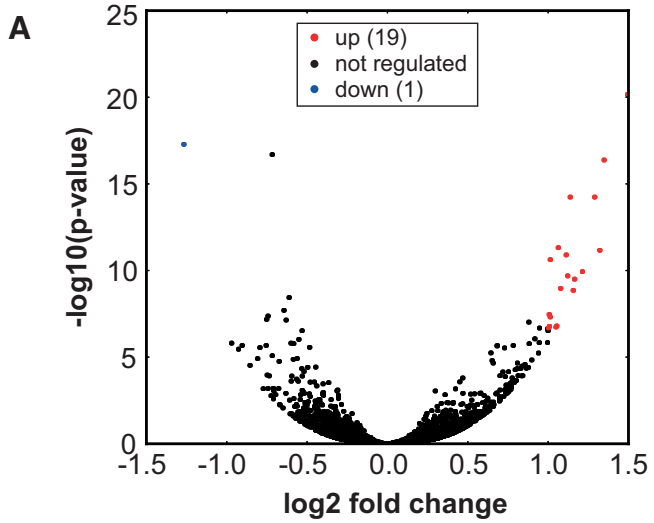

B

Gene ID	fold change	adjusted p-value
Tnfaip2	2.817	6.84E-21
Crlf1	2.547	4.18E-17
Psrc1	2.500	6.79E-12
Iqgap3	2.445	5.78E-15
Klk8	2.319	1.17E-10
Hmmr	2.242	3.15E-10
Ckap2	2.229	1.40E-09
Top2a	2.200	5.78E-18
Kif20a	2.176	2.03E-10
Lipo1	2.163	1.25E-11
Cenpf	2.111	1.08E-09
Tpx2	2.090	4.82E-12
Pbk	2.076	1.59E-07
Gm5640	2.069	1.82E-07
Mki67	2.019	2.37E-11
Prc1	2.019	4.77E-08
Kif4	2.012	1.64E-07
Kif22	2.010	3.43E-08
Fam64a	2.004	2.02E-07
Kif2c	2.000	2.97E-07
Eda2r	1.999	2.20E-07
Kdm8	1.927	2.09E-07
Nusap1	1.889	8.73E-07
Znhit3	0.416	5.20E-18

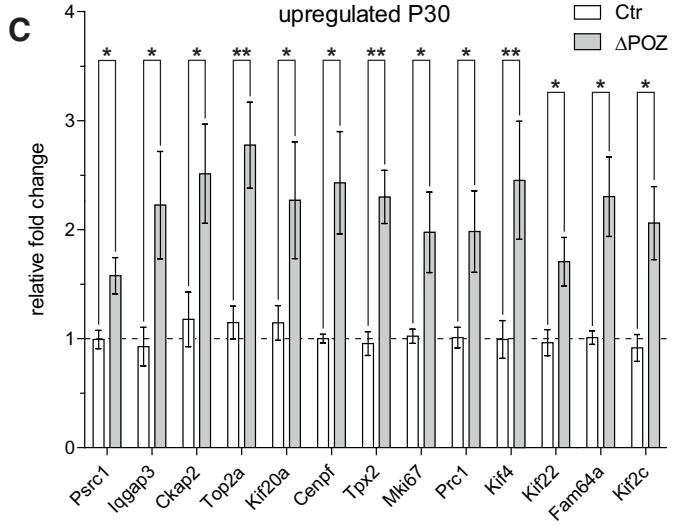

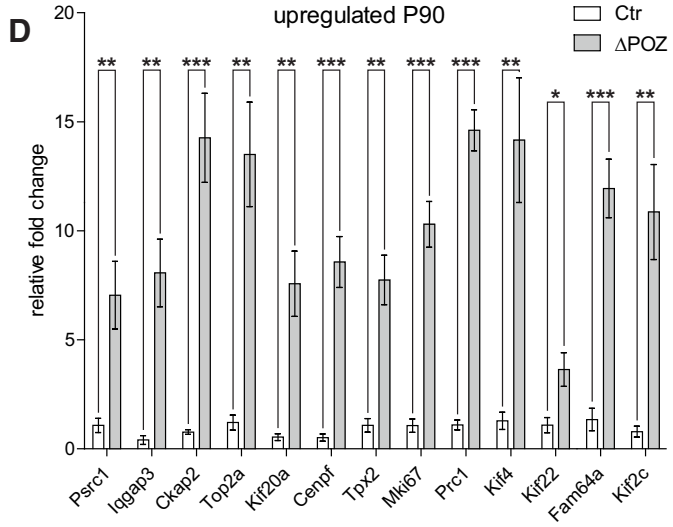

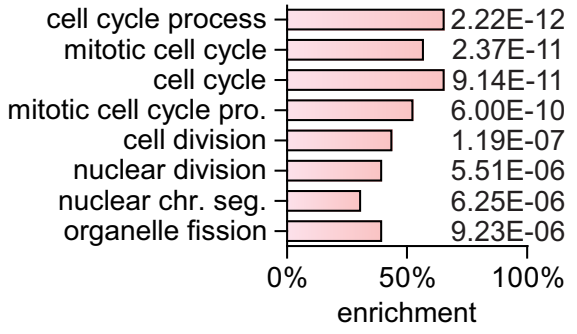

Figure 3. Identification of an early upregulated gene set implicated in cell division using RNA sequencing. ***A***, Volcano plot representing the fold change (FC) and false discovery rate-adjusted *p* value of all 19,459 considered genes in an RNA sequencing analysis conducted on P30 control (Ctr; $n = 5$) and *Miz1ΔPOZ* ($n = 3$) sciatic nerves, highlighting twofold (false discovery rate, $<10^{-6}$) regulated genes in red (up) or blue (down). ***B***, List of almost twofold deregulated genes that also have a highly significant false discovery rate of $<10^{-6}$. ***C–D***, Gene-expression analysis relative to *Gapdh,* validating a set of deregulated genes (dark red in ***B***) by qRT-PCR analysis at P30 (***C***) or P90 (***D***) in Ctr and *Miz1ΔPOZ* sciatic nerves; $n = 4$ animals per genotype and time point. ***E***, GO analysis of the deregulated gene list depicted in ***B*** representing all biological processes with $p < 10^{-5}$. ***C*** and ***D***, Asterisks indicate the results of a two-tailed, unpaired Student's t-test (*$p < 0.05$, **$p < 0.01$, ***$p < 0.001$).

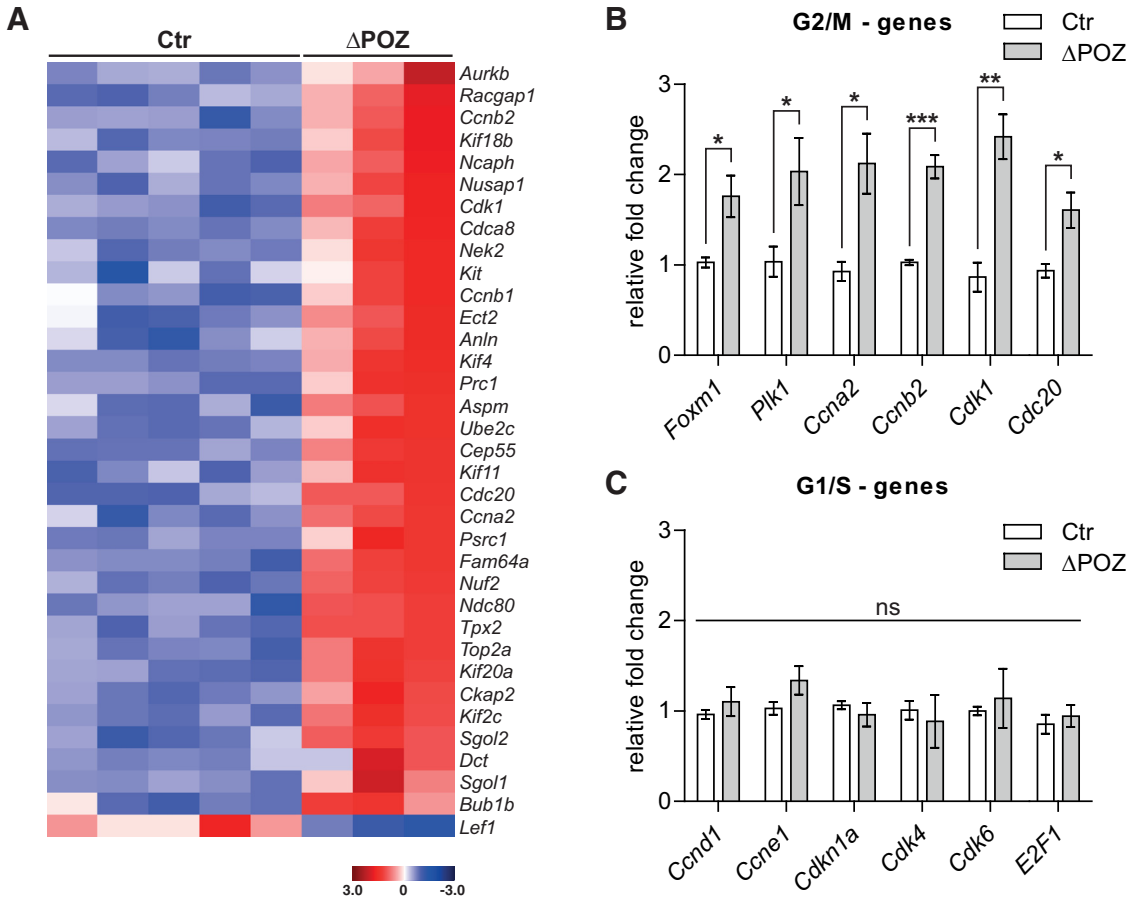

Figure 4. Upregulated genes in *Miz1ΔPOZ* sciatic nerves are associated with G2/M-progression of the cell cycle. ***A***, Heatmap illustration of all 1.5-fold deregulated genes assigned to the process "cell division" by GO ontology in each sciatic-nerve RNA sample used for RNA-Seq analysis. $n = 5$ control (Ctr) and $n = 3$ *Miz1ΔPOZ* sciatic-nerve samples. ***B***, ***C***, Expression of G2/M-associated (***B***) or G1/S-associated (***C***) genes in P30 Ctr and *Miz1ΔPOZ* sciatic-nerve samples relative to *Gapdh* determined by qRT-PCR analysis. $n = 4$ animals per genotype. ***B*** and ***C***, Asterisks indicate the results of a two-tailed, unpaired Student's t-test (*$p < 0.05$, **$p < 0.01$, ***$p < 0.001$; ns = not significant; $p > 0.05$).

there were already ~4–5 times more cycling Schwann cells in *Miz1ΔPOZ* animals compared with control animals at P30 (Fig. 5*D*). At P90, no cycling Schwann cells were detected in control mice at all, but in *Miz1ΔPOZ* mice the amount of cycling Schwann cells doubled compared with *Miz1ΔPOZ* mice at P30 (Fig. 5*D*).

Interestingly, the growth fraction of other Sox10-negative cells was similar at P30 between control and *Miz1ΔPOZ* animals (Fig. 5*E*), further indicating that the early augmented proliferation in *Miz1ΔPOZ* animals can be fully attributed to cycling Schwann cells. But while these cells completely disappeared in control animals at P60 and P90, proliferation of non-Schwann cells in *Miz1ΔPOZ* animals persisted until P60 (data not shown) and was increased at P90 (Fig. 5*E*). Proliferating cells that did not originate as Schwann cells are most likely inflammatory cells, such as macrophages (Sanz-Moreno et al., 2015), which is in accordance with the elevated expression of the macrophage marker genes *Adgre1*or *Itgam* at P60–P90 (Fig. 1*A*).

Our data show that the deletion of the Miz1 POZ domain in Schwann cells keeps a small Schwann cell population constantly in the cell cycle. This is also reflected by the GO analysis and the high percentage of regulated genes associated with the cell cycle and cell division.

The persistently cycling fraction of Schwann cells, although small, raises the question of whether the number of Schwann cells increases numerically in *Miz1ΔPOZ* mice. To test this, we counted all cells (Fig. 6*A*) and only Schwann cells (Fig. 6*B*) per area. This revealed an unchanged cell density between control and *Miz1ΔPOZ* mice at P30, P60, and P90, respectively. Only in *Miz1ΔPOZ* animals >1 year old (P400) was the cell density significantly elevated. Next, using the TUNEL assay, we tested at P60 whether there was a higher rate of apoptosis. The percentage of TUNEL-positive Schwann cells was low in both *Miz1ΔPOZ* and control animals, and did not differ between these two groups of animals (Fig. 6*C*), indicating that Schwann cell proliferation was not compensated by cell death. Finally, we measured the diameter of the sciatic nerve at P30, P90/120, and P200 and found no difference at P30, but a significantly larger diameter at P90/120 and P200 (Fig. 6*D*,*E*), indicating that a constantly increasing number of Schwann cells adds to an enlargement of the nerve diameter.

Identification of *Kdm8* and *Znhit3* as direct Miz1 target genes in *Miz1ΔPOZ* Schwann cells

To investigate a direct binding of Miz1 to the core promoter, we used MAST (Motif Alignment and Search Tool) motif analysis software (Bailey et al., 2009) to first ask whether the regulated genes listed in Figure 3*B* possess an initiator element (Do-Umehara et al., 2013) or a recently described Miz1 binding motif (Wolf et al., 2013) located ±500 bp from the transcription start site. Subsequently, we tested each individual gene that exhibited such a sequence for direct binding of Miz1 in the mouse Schwann cell line mSC80 (Boutry et

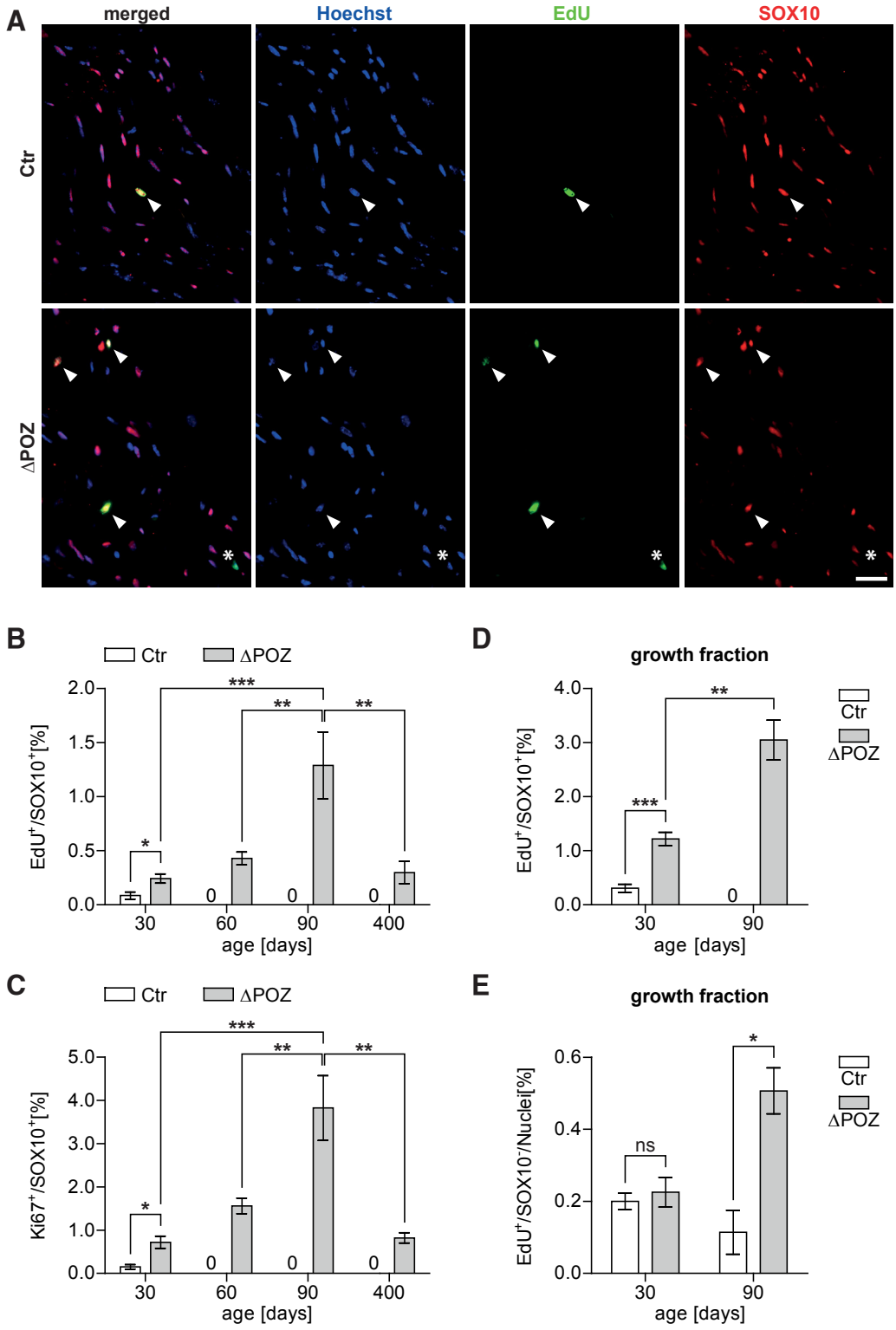

Figure 5. Sustained proliferation in *Miz1ΔPOZ* sciatic-nerve Schwann cells. ***A***, Control (Ctr) and *Miz1ΔPOZ* mice were intraperitoneally injected once with EdU and killed 1 h later. Longitudinal sections of P30 sciatic-nerve samples were costained for incorporated cell-cycle marker EdU (green) and Schwann cell marker Sox10 (red). Nuclei were counterstained using Hoechst. Arrowheads denote double-positive cells. Asterisk marks a proliferating EdU-positive, but Sox10-negative, non-Schwann cell. Scale bar, 50 μm. ***B***, Labeling index representing the percentage of Schwann cells in the cell cycle at the time of injection (EdU $^+$ and Sox10 $^+$) among all Schwann cells (Sox10 $^+$) in Ctr and *Miz1ΔPOZ* mice of indicated ages. ***C***, Quantification of the percentage of Ki67-positive Schwann cells (Sox10 $^+$) in Ctr and *Miz1ΔPOZ* mice of indicated ages. $n = 3$–5 nerves per genotype and time point; counted nuclei per nerve: 250 –700. ***D***, ***E***, Ctr and *Miz1ΔPOZ* mice at indicated ages were intraperitoneally injected seven times with EdU within 16 h and longitudinal sciatic-nerve sections were immunostained as in ***A***. ***D***, ***E***, The growth fraction was determined as the percentage of all EdU $^+$ cells during this period for Sox10 $^+$ Schwann cells (***D***) or cells of other origins (Sox10 $^-$, ***E***). $n = 3$–4 sciatic nerves per genotype; counted nuclei per nerve: 1500 –3000 at P30, 1100 –1800 at P90. ***B***, ***C***, One-way ANOVA, followed by Tukey's multiple-comparison post-test for statistical comparison among P30, P60, and P90 *Miz1ΔPOZ* mice. ***D*** and ***E*** Asterixs indicate the results of a two-tailed, unpaired Student's t-test (*$p < 0.05$, **$p < 0.01$, ***$p < 0.001$; ns = not significant; $p > 0.05$).

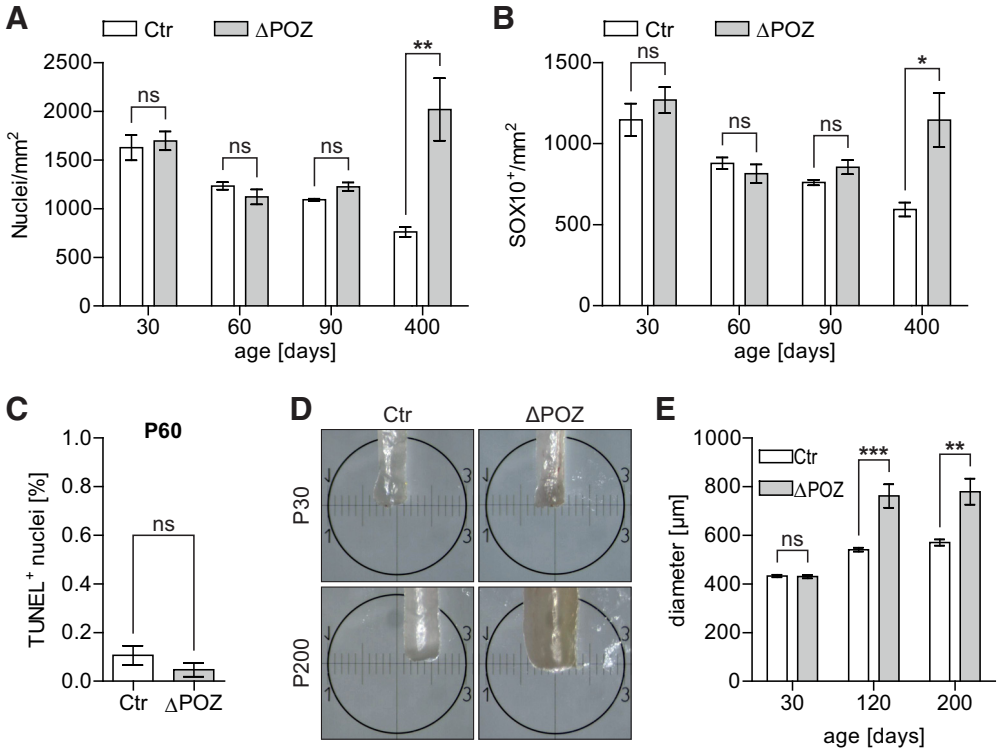

Figure 6. Sustained proliferation of *Miz1ΔPOZ* Schwann cells causes augmented nerve diameters. ***A***, ***B***, Longitudinal sections of sciatic nerves dissected at indicated ages were stained for the Schwann cell marker Sox10 and counterstained with Hoechst. Quantification of all (Hoechst $^+$) nuclei per mm^2 (***A***) or of Sox10$^+$ Schwann cells per mm^2 (***B***). $n = 3$–9 animals per genotype and time point. ***C***, TUNEL assay was performed on longitudinal sections of sciatic nerves dissected from P60 control (Ctr) and *Miz1ΔPOZ* animals using sections of an adult thymus as a positive control. Sections were counterstained with Hoechst and the percentage of TUNEL$^+$ nuclei among all nuclei was determined. $n = 4$ animals per genotype, counting 3400–5600 cells per animal. ***D***, ***E***, Representative macroscopic pictures of P30 or P200 Ctr or *Miz1ΔPOZ* sciatic nerves (***D***) and the corresponding quantification of the mean nerve diameter (***E***). The diameter was determined at three different positions throughout each individual nerve of a sciatic-nerve pair. $n = 3$–5 animals of each genotype and time point. ***A***, ***B***, ***C*** and ***E*** Asterisks indicate the results of a two-tailed, unpaired Student's t-test (*$p < 0.05$, **$p < 0.01$, ***$p < 0.001$; ns = not significant; $p > 0.05$).

al., 1992) using ChIP-qPCR with an anti-Miz1 antibody (H190, sc-22837). Primers were designed to span the binding motif and to give 80–100 bp PCR amplicons (Table 4). Furthermore, we analyzed the promoter region of the early deregulated gene *Nrg1(I)* (Frensing et al., 2008), which also appears to possess a Miz1 binding motif. From all genes tested, only the promotors from *Znhit3* and *Kdm8* revealed direct Miz1 binding (Fig. 7*A*; Table 4). This promoter occupancy appeared to be highly specific, as ChIP resulted in a >100-fold enrichment compared with an unspecific IgG control, whereas no enrichment was observed in a random region located ~1000 bp upstream from the Miz1 binding motif. Consequently, when we knocked down Miz1 in mSC80 cells by a siRNA approach, expression of *Kdm8* was upregulated, while *Znhit3* was repressed, reflecting the regulation of these genes observed in the RNAseq analysis of *Miz1ΔPOZ* sciatic nerves (Fig. 7*B*). Of note, knockdown of Miz1 in mSC80 cells did not change the expression of *Nrg1(I)* (data not shown), further confirming that this gene is not a direct Miz1 target gene.

Next, we intended to reproduce the observed binding of Miz1 to *Kdm8* and *Znhit3* in mSC80 Schwann cells *in vivo* performing ChIP qPCR on chromatin isolated from sciatic-nerve tissue of control mice at P30. Remarkably, *in vivo* binding of Miz1 to *Kdm8* and *Znhit3* could be verified (Fig. 7*C*). While current *Miz1* ChIP data are only available from biased immortalized or primary cell culture, we actually captured the highly specific interaction of Miz1 at the core promoter of *Kdm8* and *Znhit3* as it occurs in the living sciatic nerve. Additionally, the upregulation of *Kdm8* expression, as well as the repression of *Znhit3*, observed in the RNAseq experiment in *Miz1ΔPOZ* animals (Fig. 3*B*), could be confirmed by qRT-PCR on P30 sciatic nerves (Fig. 7*D*). Thus, Miz1 directly occupies a highly specific region in the promoters of *Kdm8* and *Znhit3* in Schwann cells, leading to a repression of *Kdm8* or a transactivation of *Znhit3* expression under control conditions, respectively. Bidirectional transcriptional regulation is most likely due to different binding partners recruited to Miz1 at the different promoters.

Reduced methylation of H3K36 *in vivo* correlates with increased proliferation

The yeast Hit1p is involved in the biogenesis of eukaryotic box C/D small nucleolar ribonucleoprotein particles, while the proposed function of its mammalian homolog Znhit3 is for the most part still obscure (Rothé et al., 2014). Kdm8, an H3 demethylase, is involved in the regulation of the cell cycle, most likely by regulating the expression of *Ccna1* (encoding cyclin A1) in MCF7 cells (Hsia et al., 2010) or *Cdkn1a* (encoding p21^{cip1}) in mouse embryonic fibroblasts (Ishimura et al., 2012). Knockdown experiments revealed that the absence of Kdm8 induced a G2/M block (Hsia et al., 2010), which is in line with our observation that the vast majority of the affected cell-cycle-associated genes, including *Ccna2*, *Ccnb1*, and *Ccnb2*, are involved in G2/M regulation (Fig. 4). Considering the proliferation phenotype in *Miz1ΔPOZ* Schwann cells and the impact of cyclins on cell-cycle regulation, we focused in our further experiments on *Kdm8*. Consequently, we performed Western blots to analyze the methylation status of H3K36me2, which is the proposed substrate of Kdm8 (Hsia et al., 2010). In line with the notion that *Kdm8* expression is increased

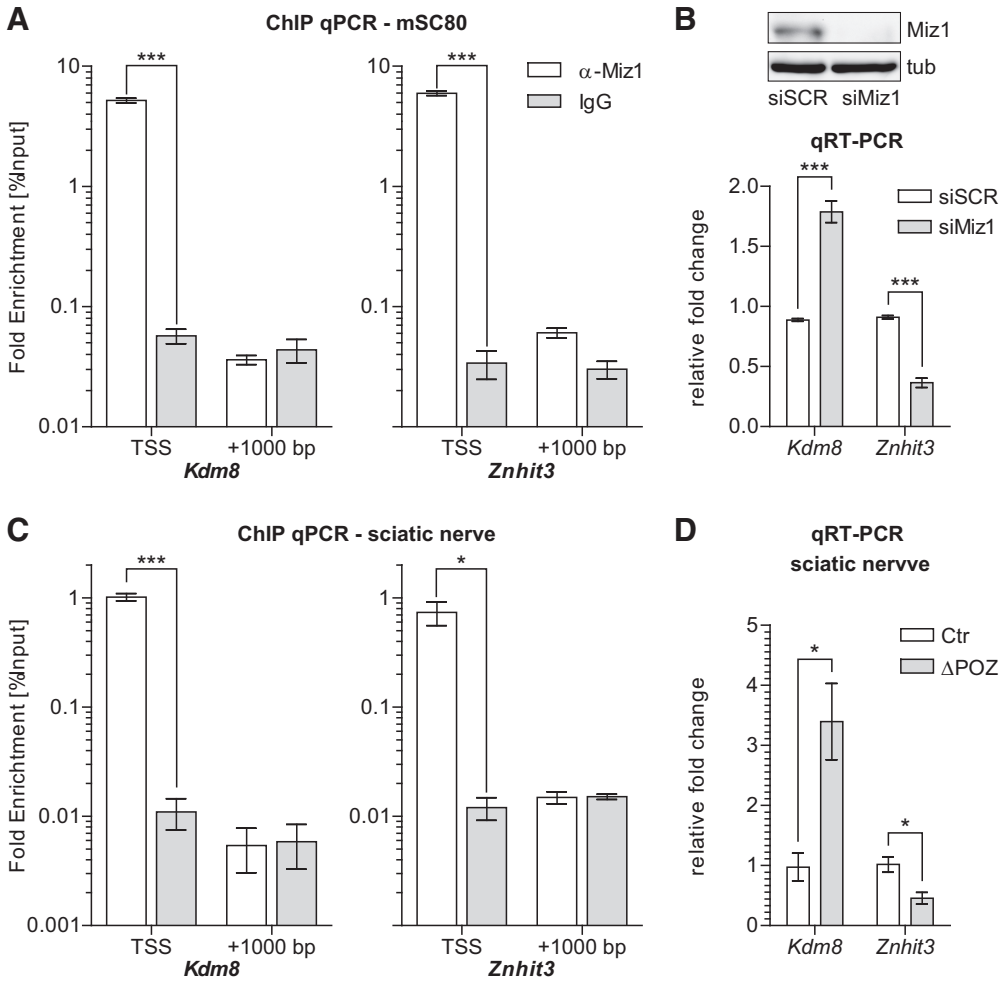

Figure 7. Identification of *Kdm8* and *Znhit3* as direct Miz1 target genes *in vitro* and *in vivo*. ***A***, *In vitro* ChIP-qPCR analysis conducted on chromatin isolated from the mSC80 Schwann cell line, using either a specific α-Miz1 antibody (H190 sc-22837) or an unspecific IgG control. Primers span either the TSS, including the Miz1 binding motif, or a randomly chosen upstream region (+1000 bp). $n = 4$ independent experiments. ***B***, RNAi-mediated Miz1 knockdown in mSC80 cells using siRNA directed against Miz1 (siMiz1) or unspecific control siRNA (siSCR). Efficient knockdown of endogenous Miz1 48 h after transfection was confirmed on Western blot using the 10E2 antibody. Gene expression of the Miz1 target genes *Kdm8* and *Znhit3* relative to *Gapdh* 48 h after siRNA transfection, determined by qRT-PCR analysis. $n = 4$ independent experiments. ***C***, *In vivo* ChIP-qPCR analysis performed on chromatin isolated from pooled sciatic nerves of 10 P30 Ctr mice, applying the same antibodies and primers as in ***A***. $n = 3$ independent experiments. ***D***, *Kdm8* and *Znhit3* gene expression measured by qRT-PCR analysis in P30 Ctr and *Miz1ΔPOZ* sciatic nerves. $n = 4$ mice per genotype. ***A–D*** Asterisks indicate the results of a two-tailed, unpaired Student's t-test (*$p < 0.05$, ***$p < 0.001$).

in nerve tissue from P30 *Miz1ΔPOZ* mice, the methylation of H3K36me2 was significantly reduced at this time point, compared with nerve tissue from age-matched control animals (Fig. 8*A*). This was confirmed by immunohistochemical staining of H3K36me2, which also showed a lower total intensity in nerve tissue from *Miz1ΔPOZ* mice, compared with control animals (Fig. 8*B*,*C*). Other common H3 methylations, such as H3K4me3 and H3K9me3, as well as total H3, were not altered at P30 in Western blots (data not shown). Moreover, it is important to note that cycling Schwann cells identified by EdU incorporation essentially lacked H3K36me2 (Fig. 8*B*,*C*). Together, these results indicate that the higher expression of *Kdm8* correlates with an attenuation of H3K36 methylation and an increased proliferation in *Miz1ΔPOZ* sciatic nerves.

To test the methylation state of deregulated genes from our list in Figure 3*B* more specifically, we performed ChIP-qPCR experiments using an antibody against H3K36^{me2}. Primers were designed to span the transcription start site (TSS) and an exon distant from the TSS of the four most highly regulated genes (*Psrc1*, *Iqgap3*, *Ckap2*, *Top2a*) related to the cell-cycle regulation. In selecting primers, the topology of H3K36me3 along a gene, which usually increases from the TSS to the 3 end (Zhang et al., 2015), was taken into consideration. Consistently, the dimethylation of H3K36 at the TSS was low in control and *Miz1ΔPOZ* nerve tissue and decreased significantly only for *Ckap2* when the Miz1 POZ domain was deleted (Fig. 8*D*). In contrast, H3K36 methylation in distant exons increased 4–5-fold in control animals, but was significantly reduced in *Miz1ΔPOZ* mice, indicating that these genes are upregulated in response to an increased demethylation at H3K36 by KDM8 specifically in the transcribed 3′ body of the gene.

Collectively, these results suggest that the exit of Schwann cells from the cell cycle is at least partially regulated by the H3K36 methylation status and KDM8. Consequently, *Kdm8* expression must be strictly regulated during physiologic postnatal Schwann cell development, when most Schwann cells enter the G0 phase. Thus, we hypothesized that *Kdm8* expression might be repressed via Miz1 and that this repression is abolished in the *Miz1ΔPOZ* situation. To test this hypothesis, we conducted qRT-PCR experiments with sciatic-nerve RNA samples from control and *Miz1ΔPOZ* animals

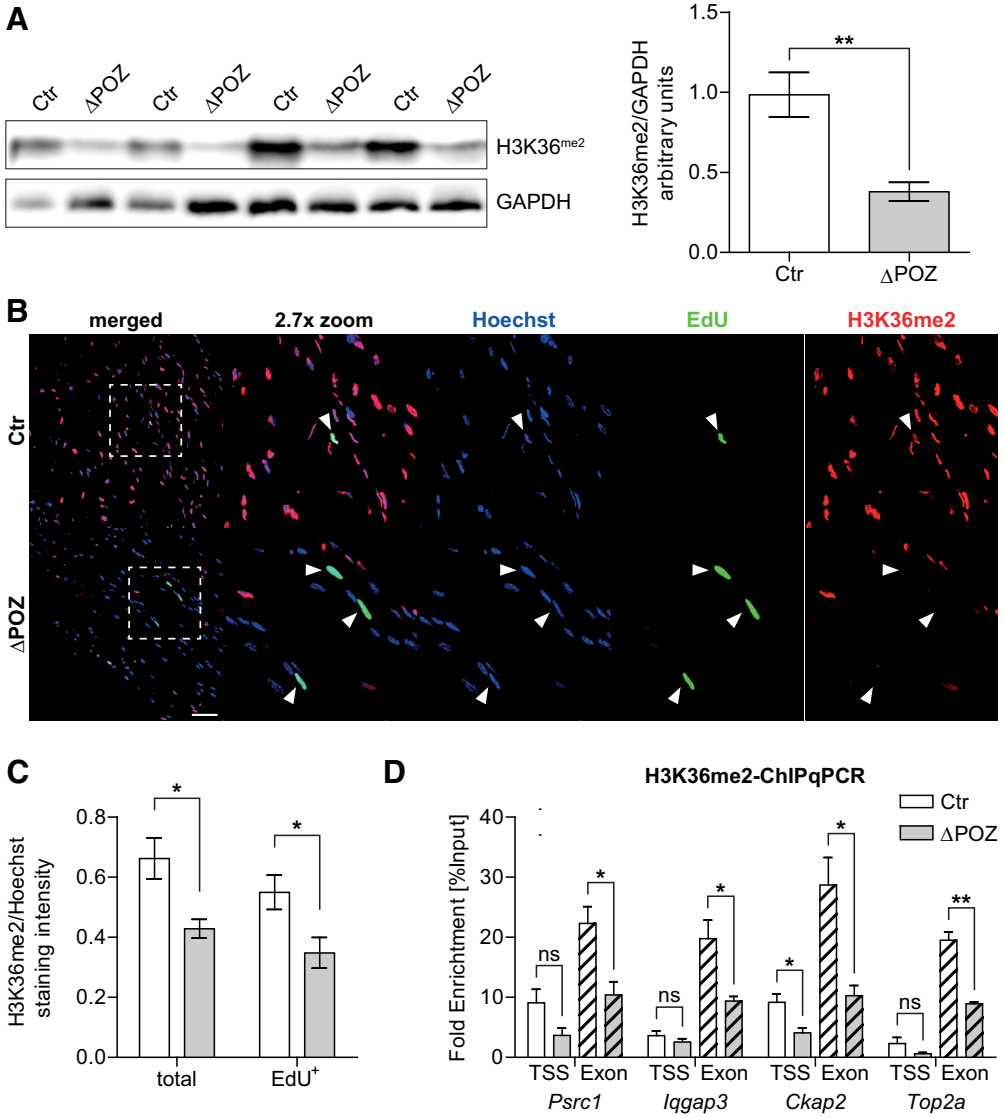

Figure 8. Decreased H3K36me2 level in *Miz1ΔPOZ* correlates with sustained proliferation. ***A***, Western blot analysis of H3K36me2 in sciatic-nerve homogenates from P30 control (Ctr) and P30 *Miz1ΔPOZ* mice and subsequent signal-intensity quantification in relation to *Gapdh* (right); $n = 4$ mice for each genotype. ***B***, P30 Ctr and *Miz1ΔPOZ* animals were intraperitoneally injected seven times with EdU within 16 h for growth-fraction analysis (Fig. 4*E*). Confocal images were taken of longitudinal sciatic-nerve sections simultaneously stained for EdU (green) and H3K36me2 (red), maintaining the same image-acquisition settings. Dashed boxes highlight magnified regions. Arrowheads, EdU-stained nuclei. Scale bar, 50 μm. ***C***, Corresponding staining-intensity quantification of confocal images representing the average H3K36 ^{me2} intensity per area in relation to the average Hoechst signal of the same area for all nuclei (total) or only for EdU-positive nuclei (EdU $^{+}$). $n =$ 4 mice per genotype; analyzed nuclei: $\geq$1000 per sample. ***D***, *In vivo* ChIP-qPCR analysis conducted on chromatin isolated from pooled sciatic nerves of 10 P30 Ctr or *Miz1ΔPOZ* mice using an H3K36me2 antibody and primers spanning a region close to the TSS or a coding region at the 3′ end of the indicated genes. For most genes and regions, an average fold enrichment compared with an unspecific IgG control $>$100, but at least 20 confirmed specificity in each experiment (data not shown). $n = 3$ independent experiments. ***A***, ***C*** and ***D*** Asterisks indicate the results of a two-tailed, unpaired Student's t-test (*$p < 0.05$, **$p < 0.01$; ns = not significant).

at different stages during postnatal development (P2.5, P7.5, P15, and P30) and analyzed *Kdm8*-expression levels over time. This analysis affirmed that *Kdm8* levels were continuously repressed in control nerve tissue starting at P7.5 (Fig. 9*A*). Interestingly, at the same time point Miz1 gene (*Zbtb17*) expression transiently increased (Fig. 9*A*). In contrast, nerves depleted of functional Miz1 failed to reduce the initial *Kdm8*-expression status, resulting in a slight accumulation of *Kdm8* mRNA (Fig. 9*A*).

Surprisingly, this did not translate into a significantly reduced H3K36me2 level before P30 (Figs. 8*A*, 9*B*). For that reason, we analyzed the expression of the H3K36 methyltransferases Nsd1, Nsd2, and Nsd3 during postnatal development in control mice (Wagner and Carpenter, 2012). The expression of Nsd1 increased slightly but not significantly during normal postnatal development, while Nsd3 peaked at P7.5 and Nsd2 was robustly repressed at P15 and P30 (Fig. 9*C*). Together with the time course of *Kdm8* expression (Fig. 9*A*), these data suggest that H3K36 methylation participates in normal postnatal development of peripheral nerves in a complex manner that is not exclusively regulated by Kdm8. However, in our RNAseq analysis and supporting qRT-PCR experiments from P30 (data not shown), the expression of Nsd1–Nsd3, as well as the expression of other enzymes with a

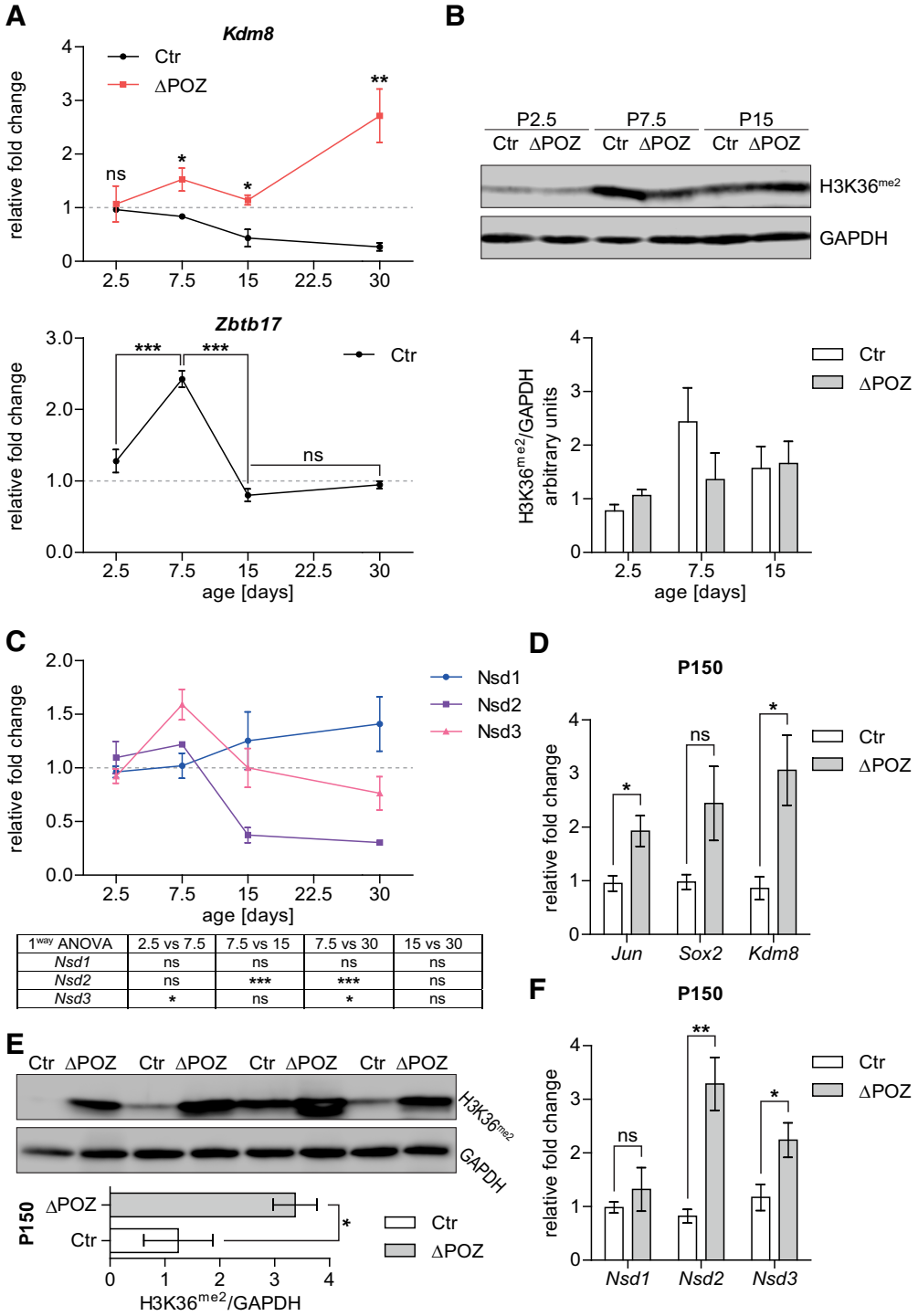

Figure 9. H3K36 methylation is regulated in a complex manner during Schwann cell development. ***A***, Expression analysis of *Kdm8* and the Miz1 gene (*Zbtb17*) relative to *Gapdh* in control (Ctr) or *Miz1ΔPOZ* sciatic nerves, determined by qRT-PCR analysis at indicated time points during postnatal peripheral nerve development. Asteriks in the lower graph are results of an one-way ANOVA statistical analysis, followed by Tukey's multiple-comparison post-test. $n = 3$ mice per genotype and time point. ***B***, Representative Western blot showing the H3K36 methylation in sciatic-nerve homogenates from P2.5, P7.5, and P15 Ctr and *Miz1ΔPOZ* mice, respectively, and a signal-intensity quantification relative to *Gapdh* (right); $n = 3$ mice for each genotype. ***C***, Gene expression of H3K36-specific histone methyltransferases *Nsd1–3* relative to *Gapdh* using qRT-PCR analysis on RNA from Ctr sciatic nerves dissected at indicated ages. Results of the one-way ANOVA statistical analysis, followed by Tukey's multiple-comparison post-test, are represented in the table below. $n = 3$ mice per time point. ***D***, H3K36me2 Western blot analysis in sciatic-nerve homogenates from P150 Ctr and *Miz1ΔPOZ* mice and subsequent signal-intensity quantification relative to *Gapdh*. $n = 4$ mice per genotype. ***E***, ***F***, Expression analysis of dedifferentiation-associated genes *Jun* and *Sox2* as well as *Kdm8* (***E***) or histone methyltransferases *Nsd1–3* (***F***) relative to *Gapdh* using qRT-PCR analysis on RNA from P150 Ctr and *Miz1ΔPOZ* sciatic nerves. $n = 4$ mice per genotype and time point. ***A*** (upper graph) and ***D-F*** Asterisks indicate the results of a two-tailed, unpaired Student's t-test. ***A*** (lower panel) and ***C*** Results of the one-way ANOVA statistical analysis, followed by Tukey's multiple-comparison post-test (*$p < 0.05$, **$p < 0.01$, ***$p < 0.001$; ns = not significant).

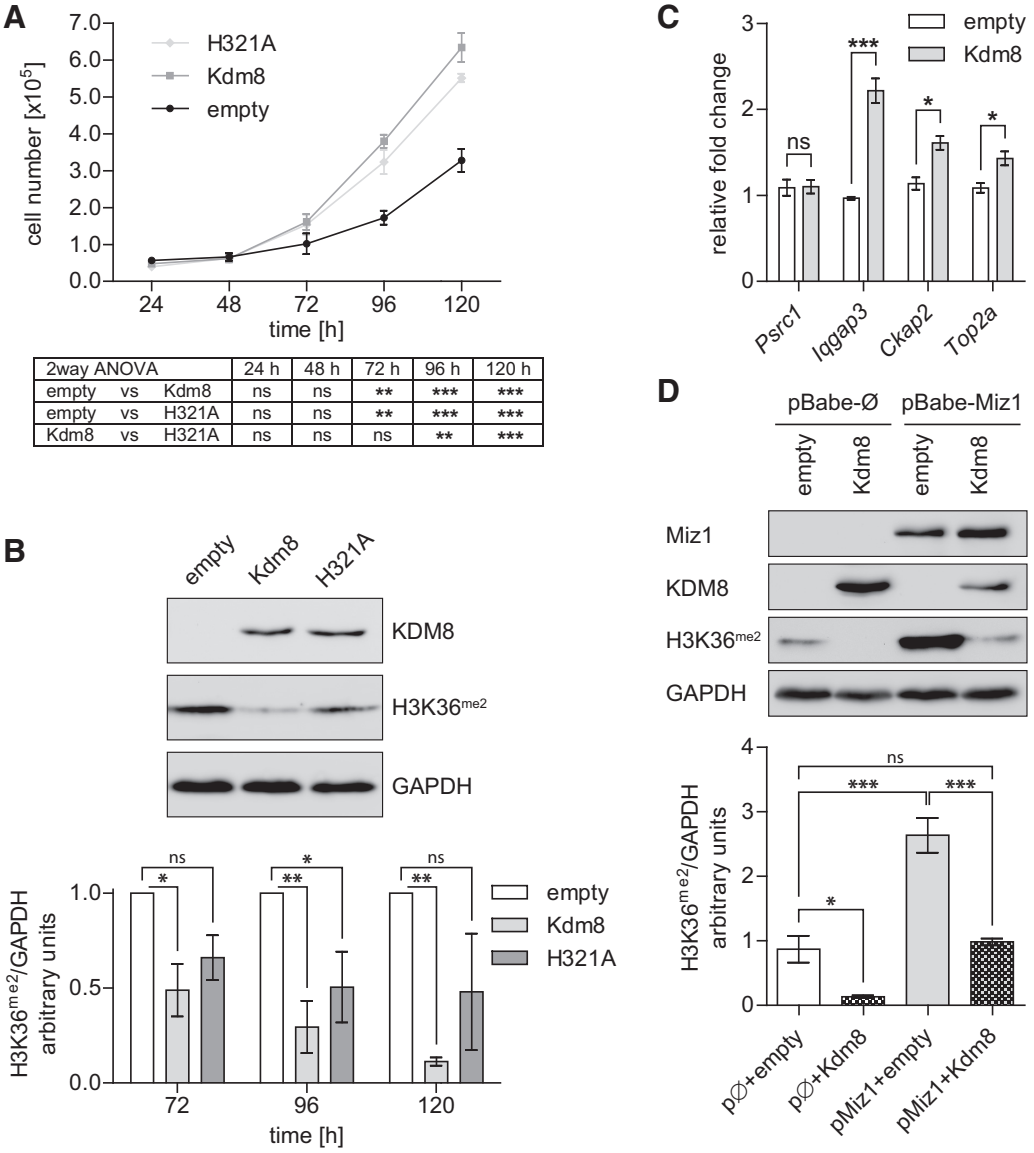

2way ANOVA			24 h	48 h	72 h	96 h	120 h
empty	vs	Kdm8	ns	ns	**	***	***
empty	vs	H321A	ns	ns	**	***	***
Kdm8	vs	H321A	ns	ns	ns	**	***

Figure 10. Kdm8 promotes mSC80 Schwann cell proliferation likely through H3K36 demethylation. ***A***, Amido black assay for cell-number quantification of mSC80 Schwann cells at indicated times after transfection with *empty*, *Kdm8*, or *KDM8H321A* plasmids. Results of a two-way ANOVA statistical analysis followed by a Bonferroni's post-tests are depicted in the table below. $n = 4$ individual experiments. ***B***, Representative Western blot of Kdm8 (detected by a Myc-Tag antibody) and H3K36 ^{me2} protein levels in mSC80 cell homogenates 72 h after transfection with the indicated plasmids (top). Signal intensity quantification of H3K36me2 at indicated times after transfection (bottom). $n = 4$ (72 h), 3 (96 h), and 2 (120 h) individual experiments. Statistical test: two-way ANOVA, followed by Bonferroni's post-tests. ***C***, Gene expression analysis of cycle-associated genes shown to be differentially methylated in *Miz1ΔPOZ* mice (Fig. 8*D*) relative to *Gapdh* using qRT-PCR analysis on RNA from mSC80 cells 72 h after transfection with *empty* or *Kdm8* plasmids. One of two independent experiments is shown using $n = 3$ replicates per condition in each experiment. ***D***, Representative Western blot stained for Miz1, Kdm8 (Myc-Tag) and H3K36 ^{me2} 72 h after transfection of stably Miz1 or empty pBabe vector-expressing mSC80 Schwann cells with another empty or Kdm8 vector (top). Signal-intensity quantification of H3K36me2 of $n = 3$ independent experiments is presented at the bottom. Statistical test: one-way ANOVA, followed by Tukey's multiple-comparison post test. ***A*** and ***B*** Asterisks indicate the results of a two-way ANOVA statistical analysis followed by a Bonferroni's post-test ***C***, Asterisks indicate the results of a two-tailed, unpaired Student's *t*-test. ***D***, Statistical test: one-way ANOVA, followed by Tukey's multiple comparisonpost test (*$p < 0.05$, **$p < 0.01$, ***$p < 0.001$; ns = not significant).

proven *in vivo* H3K36 methyltransferase activity (Wagner and Carpenter, 2012), was not altered. Nor did any other reported lysine-specific histone demethylase than Kdm8 (Kdm1–Kdm6) show any expression changes at P30. Together, our data suggest that the demethylation of H3K36 in *Miz1ΔPOZ* nerve tissue is predominantly caused by higher expression of *Kdm8*.

At P150, when the acute phase is abated and clinically symptoms are hardly visible, attenuated demyelination, as well as hypomyelinated axons, are still observed (Sanz-Moreno et al., 2015), indicating that regeneration is compensating for ongoing myelin destruction. This is underlined by the expression of dedifferentiation genes, such as *Jun*, *Sox2*, or *Nrg1(I)*, which were still elevated at P150 in *Miz1ΔPOZ* animals (Fig. 9*D*). Also, Kdm8 expression remained higher than normal at this time point in the knock-out mice (Fig. 9*D*). Intriguingly, H3K36 methylation increased threefold in *Miz1ΔPOZ* animals compared with control animals (Fig. 9*E*). This prompted us to measure the expression of H3 methyltransferases with a proven *in vivo* K36 methylase activity (Wagner and Carpenter, 2012) at P150. While *Setmar* and *SetD2* expression was not detectable (data not shown), we found *Nsd1* unchanged, but the expression of *Nsd2* and *Nsd3* significantly increased (Fig. 9*F*). Whether the activity of the methyltransferases overwrite the demethylase activity or whether there are different Schwann cell populations representing a degenera-

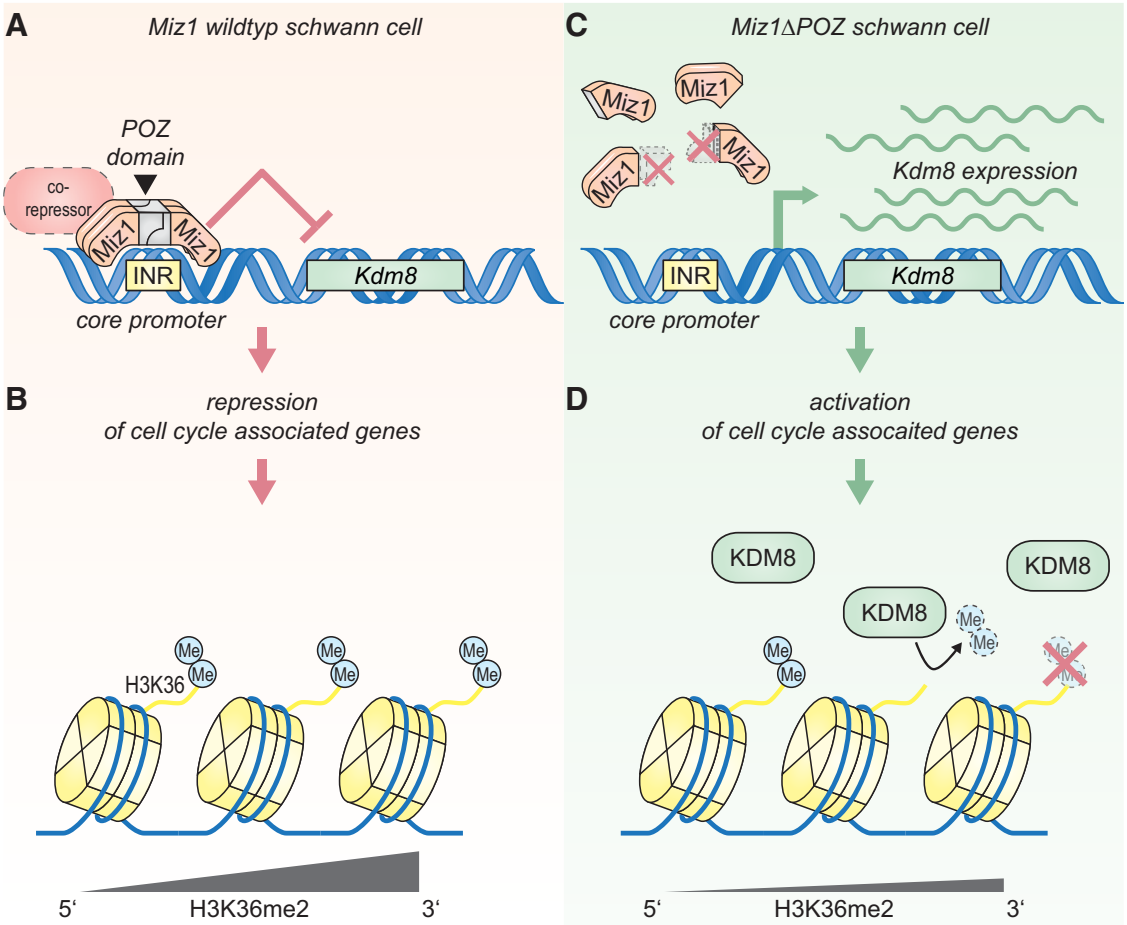

Figure 11. Model of the Miz1 and Kdm8 interplay and its impact on Schwann cell proliferation by modulation of the H3K36 ^{me2} status. ***A***, Miz1 represses *Kdm8* expression in Schwann cells directly at its initiator (INR) region via a conserved binding sequence (Wolf et al., 2013). According to established models, this repression requires a corepressor, which so far remains unknown. ***B***, Reduction of Kdm8 levels during postnatal peripheral nerve development correlates with the exit of Schwann cells from the cell cycle and is in part regulated through preserved H3K36 ^{me2} histone marks, especially at the transcribed 3′ gene body of cell-cycle-associated genes. ***C***, Deletion of the Miz1 POZ domain in *Miz1ΔPOZ* Schwann cells abolishes its gene-repression function and releases *Kdm8* expression. ***D***, Increased Kdm8 levels result in augmented H3K36 demethylation, particularly at the transcribed 3′ gene body of cell-cycle-associated genes, hindering some *Miz1ΔPOZ* Schwann cells from exiting the cell cycle or allowing G0 Schwann cells to re-enter the cell cycle.

tive (with high *Kdm8* expression) or regenerative (with high methyltransferase expression) phenotype remains to be elucidated. Finally, at P300, no difference in H3K36 methylation could be detected between *Miz1ΔPOZ* and control animals (data not shown).

H3K36 demethylation causes hyperproliferation of mSC80 cells

To verify our *in vivo* findings and to underline that the regulatory mechanisms can be attributed to Schwann cells, we transfected the mouse Schwann cell line mSC80 either with wild-type *Kdm8* or with the mutant *Kdm8H321A* (Huang et al., 2015) and analyzed their effects on proliferation. As expected from our *in vivo* results, Schwann cells overexpressing *Kdm8* doubled their cell number compared with mock-transfected cells over 5 d and this effect was significantly diminished when *Kdm8H321A* was transfected (Fig. 10*A*). To confirm exogenous KDM8 expression and to elaborate whether the induction of proliferation by *Kdm8* overexpression was attended by a reduction of H3K36me2, we also collected samples for protein analysis. Western blots indicated robust Kdm8 expression and revealed a subsequent reduction of H3K36me2 72 h after transfection (Fig. 10*B*, top), notably, the time when increased proliferation becomes initially visible (Fig. 10*A*). Consistently, H3K36me2 levels remained low in Kdm8 samples 96 and 120 h after transfection, but to a weaker degree in Kdm8H321A-expressing cells (Fig. 10*B*, bottom). In addition, some genes differently methylated in control and Miz1POZ nerve tissue (Fig. 8*D*) are expressed more highly in mSC80 cells overexpressing Kdm8 (Fig. 10*C*). Finally, we asked whether overexpression of Miz1 results in an induction of H3K36 methylation via specific *Kdm8* repression, and whether the initial H3K36 methylation status might be restored by coexpression of an exogenous *Kdm8* construct. Western blot analysis showed that Miz1 overexpression effectively increased H3K36 methylation (Fig. 10*D*, lane 3). This was abolished when Kdm8 was coexpressed, suggesting, together with the *in vivo* data, that usually *Kdm8* is repressed by Miz1 and that its demethylase activity is regulating cell proliferation via the H3K36 dimethylation status.

Discussion

In a recent paper, we described the clinically acute phase of a demyelinating late-onset neuropathy in mice that harbor a deletion of the POZ domain of the transcription factor Miz1 in Schwann cells (Sanz-Moreno et al., 2015). To understand the initial molecular disorder in *Miz1ΔPOZ* sciatic nerves, we traced back the first gene regulatory changes to P30. Notably, the postnatal development of the peripheral nervous system in mice at this time is finished (Svaren

and Meijer, 2008) and the ultrastructure of myelinated fibers in *Miz1ΔPOZ* animals is still normal (Sanz-Moreno et al., 2015). RNAseq analysis at P30 revealed a small set of genes deregulated >2-fold in *Miz1ΔPOZ* mice, most of which are upregulated and involved in cell-cycle regulation. In line with this observation, we found that a proportion of Schwann cells failed to exit or re-entered the cell cycle in *Miz1ΔPOZ* animals, while in control animals, no cycling of Schwann cells as late as P45 could be detected.

Among the early deregulated genes in *Miz1ΔPOZ* nerve tissue is the neurotrophic factor neuregulin 1 (Ngr1), which has important impact on Schwann cell proliferation and differentiation (Mei and Nave, 2014). Nrg1 occurs in different isoforms (Nave and Salzer, 2006). Previous studies have shown that Nrg1 (II) signaling causes demyelination in mature nerves (Zanazzi et al., 2001) and that Nrg1 (III) plays an important role in axon myelination (Michailov et al., 2004). In P30 *Miz1ΔPOZ* sciatic nerves, Nrg1 (II) was undetectable and Nrg1 (III) was unchanged (data not shown), suggesting that they are not implicated in the initiation of demyelination or Schwann cell proliferation in *Miz1ΔPOZ* nerves. On the other hand, Stassart et al. could not detect developmental differences in mice overexpressing Nrg1 (I) or deficient for Nrg1 (I) and provided a model in which Nrg1 (I) is expressed by Schwann cells upon loss of axonal contact (Stassart et al., 2013). The precise role of Nrg1 (I) in our model remains to be elucidated.

Both genes have previously been identified in a ChIP-Seq analysis among 261 high-affinity Miz1 target genes in neurospheres (Wolf et al., 2013), highlighting conserved promoter occupancy.

Kdm8/Jdmd5 is a reported member of the H3 *JumonjiC* (JmjC) domain histone demethylase family with a proposed specificity to H3K36^{me2} (Klose et al., 2006; Kooistra and Helin, 2012). Various researchers have implicated KDM8 in the regulation of cell proliferation in tumors (Hsia et al., 2010; Zhao et al., 2015) and in the context of cell development (Ishimura et al., 2012; Zhu et al., 2014). But the mechanism that enables KDM8 to actually promote proliferation is still a topic of controversy. It was initially proposed that an increased expression of *Cyclin A1*, in response to an augmented H3K36^{me2} demethylation, causes a higher proliferation in MCF7 cells (Hsia et al., 2010). Other proposed mechanisms include the transcriptional repression of *Cdkn1a* via its methylation status (Ishimura et al., 2012) or a demethylase-independent regulatory pathway, for example through physical interaction with the tumor suppressor p53 (Huang et al., 2015). Our results strongly suggest that increased *Kdm8* expression in *Miz1ΔPOZ* sciatic nerves results in a reduction of H3K36me2. In control as well as in *Miz1ΔPOZ* nerves, H3K36me2 was reduced in EdU-positive cells, indicating a correlation of the H3K36 methylation status and proliferation. In line with this observation, overexpression of KDM8 in the mouse Schwann cell line mSC80 reduced H3K36^{me2} and enhanced proliferation, and this was attenuated when an enzymatically compromised Kdm8 mutant was used. In a corresponding experiment, overexpression of Miz1 increased H3K36^{me2} and a simultaneous overexpression of KDM8 was sufficient to almost completely restore initial H3K36^{me2} levels. The inhibitory function of Miz1 on *Kdm8* expression and subsequent proliferation implies that Miz1 is required during normal Schwann cell development to ensure proper cell-cycle exit. In line with this notion, Kdm8 was continuously reduced in control sciatic-nerve tissue during postnatal development from P7.5 on, compared with *Miz1ΔPOZ* animals in which Kdm8 increased slightly. This repression correlates with the period of the final and entire exit of Schwann cells from the cell cycle, which is completed at P30 in the rat (Stewart, 1993).

Epigenetic chromatin modifications have been described as an important feature in the regulation of Schwann cell differentiation. The impact of chromatin remodeling (Witkowski and Foulkes, 2015) in the differentiation of this cell type has been shown for SWI/SNF (SWItch/Sucrose Non-Fermentable; Weider et al., 2012; Limpert et al., 2013) or the NurD (Hung et al., 2012) complex. Also, histone deacetylases play key roles during Schwann cell myelination (Chen et al., 2011; Jacob et al., 2011; Hung et al., 2012, 2015). In the case of histone methylation, it was shown that the high expression of the H3K27me3 demethylase Kdm6B/Jmjd3 in Schwann cells activates the Ink4a/Arf locus and thus switches off proliferation (Gomez-Sanchez et al., 2013). Further, the methyltransferase *polycomb repressive complex 2* (*PCR2*) catalyzes H3K27 methylation and, when the PCR2 subunit Eed is deleted in Schwann cells, the thickness of myelin is reduced (Ma et al., 2015, 2016). Interestingly, H3K27 hypomethylation does not change the expression of c-Jun, indicating that under these circumstances the usual injury repair program is not activated. Conversely, in *Miz1ΔPOZ* Schwann cells we observed a continuously elevated expression of the histone demethylase Kdm8/Jmjd5 with a specificity to H3K36me2 (Kooistra and Helin, 2012). Our *in vivo* ChIP-qPCR analysis on chromatin from sciatic-nerve tissue with an antibody against H3K36^{me2} could, for example, show that show for the cell-cycle-related genes *Psrc1*, *Iqgap3*, *Ckap2*, and *Top2a* that H3K36^{me2} is increasingly distributed toward the 3′ transcribed body in control animals. In contrast, *Miz1ΔPOZ* mice revealed decreased H3K36^{me2} levels in these genes, especially in the transcribed gene body, indicating a specific demethylation by KDM8 (Zhang et al., 2015). Thus, the linkage between elevated *Kdm8* expression, hypomethylation of H3K36 from cell-cycle-relevant genes, and the option of adult Schwann cells to re-enter the cell cycle suggests that the release of *Kdm8* repression in the absence of a functional Miz1 is a central issue in the pathogenesis of the *Miz1ΔPOZ* neuropathy.

In the original model concerning the function of Miz1, researchers postulated that a transactivating activity in complex with Npm1 at P300 is inhibited when other binding partners, such as Myc, Bcl6, Gfi or Zbtb4, join the complex (Herkert and Eilers, 2010). Which binding partner confers repression of *Kdm8* by Miz1 remains to be elucidated. We propose a model in which the Miz1 tetramer (Stogios et al., 2005; Kosan et al., 2010; Stead and Wright, 2014) represses *Kdm8* expression together with a so-far-unknown corepressor (Fig. 11*A*). As a consequence, cell-cycle-associated genes, such as *Psrc1*, *Iqgap3*, *Ckap2*, and *Top2a*, are repressed by preservation of H3K36^{me2} in the 3′ gene body, thereby enforcing the G0 arrest of the entire Schwann cell population (Fig. 11*B*). The deletion of the Miz1 POZ domain abrogates Miz1 tetramerization and subsequent DNA binding. As a result, *Kdm8* gene expression is released from Miz1-transcriptional inhibition in *Miz1ΔPOZ* Schwann cells (Fig. 11*C*). We propose that the release of *Kdm8* repression in the absence of a functional Miz1 results in a H3K36 hypomyelination and insufficient epigenetic repression of cell-cycle-associated genes (Fig. 11*D*). To our knowledge, this is the first time that the methylation status of H3K36 is linked to the pathogenesis of a peripheral neuropathy, extending the disease-related epigenetic changes in Schwann cells.

References

Adhikary S, Peukert K, Karsunky H, Beuger V, Lutz W, Elsässer HP, Möröy T, Eilers M (2003) Miz1 is required for early embryonic development during gastrulation. Mol Cell Biol 23:7648–7657. CrossRef Medline

Bailey TL, Boden M, Buske FA, Frith M, Grant CE, Clementi L, Ren J, Li WW, Noble WS (2009) MEME Suite: tools for motif discovery and searching. Nucleic Acids Res 37:W202–W208. CrossRef Medline

Boutry JM, Hauw JJ, Gansmüller A, Di-Bert N, Pouchelet M, Baron-Van Evercooren A (1992) Establishment and characterization of a mouse Schwann cell line which produces myelin *in vivo*. J Neurosci Res 32:15–26. CrossRef Medline

Chen Y, Wang H, Yoon SO, Xu X, Hottiger MO, Svaren J, Nave KA, Kim HA, Olson EN, Lu QR (2011) HDAC-mediated deacetylation of NF-κB is critical for Schwann cell myelination. Nat Neurosci 14:437–441. CrossRef Medline

Combes G, Alharbi I, Braga LG, Elowe S (2017) Playing polo during mitosis: PLK1 takes the lead. Oncogene 36:4819–4827. CrossRef Medline

Dobin A, Davis CA, Schlesinger F, Drenkow J, Zaleski C, Jha S, Batut P, Chaisson M, Gingeras TR (2013) STAR: ultrafast universal RNA-seq aligner. Bioinformatics 29:15–21. CrossRef Medline

Do-Umehara HC, Chen C, Urich D, Zhou L, Qiu J, Jang S, Zander A, Baker MA, Eilers M, Sporn PH, Ridge KM, Sznajder JI, Budinger GR, Mutlu GM, Lin A, Liu J (2013) Suppression of inflammation and acute lung injury by Miz1 via repression of C/EBP-δ. Nat Immunol 14:461–469. CrossRef Medline

Frensing T, Kaltschmidt C, Schmitt-John T (2008) Characterization of a neuregulin-1 gene promoter: positive regulation of type I isoforms by NF-kappaB. Biochim Biophys Acta 1779:139–144. CrossRef Medline

Fuhrmann D, Elsässer HP (2015) Schwann cell Miz without POZ: degeneration meets regeneration. Neural Regen Res 10:1563–1564. CrossRef Medline

Gebhardt A, Kosan C, Herkert B, Möröy T, Lutz W, Eilers M, Elsässer HP (2007) Miz1 is required for hair follicle structure and hair morphogenesis. J Cell Sci 120:2586–2593. CrossRef Medline

Gomez-Sanchez JA, Gomis-Coloma C, Morenilla-Palao C, Peiro G, Serra E, Serrano M, Cabedo H (2013) Epigenetic induction of the Ink4a/Arf locus prevents Schwann cell overproliferation during nerve regeneration and after tumorigenic challenge. Brain 136:2262–2278. CrossRef Medline

Herkert B, Eilers M (2010) Transcriptional repression: the dark side of myc. Genes Cancer 1:580–586. CrossRef Medline

Hönnemann J, Sanz-Moreno A, Wolf E, Eilers M, Elsässer HP (2012) Miz1 is a critical repressor of cdkn1a during skin tumorigenesis. PloS One 7:e34885. CrossRef Medline

Hsia DA, Tepper CG, Pochampalli MR, Hsia EY, Izumiya C, Huerta SB, Wright ME, Chen HW, Kung HJ, Izumiya Y (2010) KDM8, a H3K36me2 histone demethylase that acts in the cyclin A1 coding region to regulate cancer cell proliferation. Proc Natl Acad Sci U S A 107:9671–9676. CrossRef Medline

Huang X, Zhang S, Qi H, Wang Z, Chen HW, Shao J, Shen J (2015) JMJD5 interacts with p53 and negatively regulates p53 function in control of cell cycle and proliferation. Biochim Biophys Acta 1853:2286–2295. CrossRef Medline

Hung H, Kohnken R, Svaren J (2012) The nucleosome remodeling and deacetylase chromatin remodeling (NuRD) complex is required for peripheral nerve myelination. J Neurosci 32:1517–1527. CrossRef Medline

Hung HA, Sun G, Keles S, Svaren J (2015) Dynamic regulation of Schwann cell enhancers after peripheral nerve injury. J Biol Chem 290:6937–6950. CrossRef Medline

Ishimura A, Minehata K, Terashima M, Kondoh G, Hara T, Suzuki T (2012) Jmjd5, an H3K36me2 histone demethylase, modulates embryonic cell proliferation through the regulation of Cdkn1a expression. Development 139:749–759. CrossRef Medline

Ito S, Karnovsky WJ (1968) Formaldehyde-glutaraldehyde fixatives containing trinitro compounds. J Cell Biol 39:168a–169a.

Jacob C, Christen CN, Pereira JA, Somandin C, Baggiolini A, Lötscher P, Ozçelik M, Tricaud N, Meijer D, Yamaguchi T, Matthias P, Suter U (2011) HDAC1 and HDAC2 control the transcriptional program of myelination and the survival of Schwann cells. Nat Neurosci 14:429–436. CrossRef Medline

Jessen KR, Mirsky R (2005) The origin and development of glial cells in peripheral nerves. Nat Rev Neurosci 6:671–682. CrossRef Medline

Jessen KR, Mirsky R (2016) The repair Schwann cell and its function in regenerating nerves. J Physiol 594:3521–3531. CrossRef Medline

Jordan M, Schallhorn A, Wurm FM (1996) Transfecting mammalian cells: optimization of critical parameters affecting calcium-phosphate precipitate formation. Nucleic Acids Res 24:596–601. CrossRef Medline

Klose RJ, Kallin EM, Zhang Y (2006) JmjC-domain-containing proteins and histone demethylation. Nat Rev Genet 7:715–727. CrossRef Medline

Kooistra SM, Helin K (2012) Molecular mechanisms and potential functions of histone demethylases. Nat Rev Mol Cell Biol 13:297–311. CrossRef Medline

Kosan C, Saba I, Godmann M, Herold S, Herkert B, Eilers M, Möröy T (2010) Transcription factor miz-1 is required to regulate interleukin-7 receptor signaling at early commitment stages of B cell differentiation. Immunity 33:917–928. CrossRef Medline

Limpert AS, Bai S, Narayan M, Wu J, Yoon SO, Carter BD, Lu QR (2013) NF-κB forms a complex with the chromatin remodeler BRG1 to regulate Schwann cell differentiation. J Neurosci 33:2388–2397. CrossRef Medline

Livak KJ, Schmittgen TD (2001) Analysis of relative gene expression data using real-time quantitative PCR and the 2(-Delta Delta C(T)) Method. Methods 25:402–408. CrossRef Medline

Love MI, Huber W, Anders S (2014) Moderated estimation of fold change and dispersion for RNA-seq data with DESeq2. Genome Biol 15:550. CrossRef Medline

Ma KH, Hung HA, Srinivasan R, Xie H, Orkin SH, Svaren J (2015) Regulation of peripheral nerve myelin maintenance by gene repression through polycomb repressive complex 2. J Neurosci 35:8640–8652. CrossRef Medline

Ma KH, Hung HA, Svaren J (2016) Epigenomic regulation of Schwann cell reprogramming in peripheral nerve injury. J Neurosci 36:9135–9147. CrossRef Medline

Mei L, Nave KA (2014) Neuregulin-ERBB signaling in the nervous system and neuropsychiatric diseases. Neuron 83:27–49. CrossRef Medline

Michailov GV, Sereda MW, Brinkmann BG, Fischer TM, Haug B, Birchmeier C, Role L, Lai C, Schwab MH, Nave KA (2004) Axonal neuregulin-1 regulates myelin sheath thickness. Science 304:700–703. CrossRef Medline

Möröy T, Saba I, Kosan C (2011) The role of the transcription factor Miz-1 in lymphocyte development and lymphomagenesis-binding Myc makes the difference. Semin Immunol 23:379–387. CrossRef Medline

Nave KA, Salzer JL (2006) Axonal regulation of myelination by neuregulin 1. Curr Opin Neurobiol 16:492–500. CrossRef Medline

Nowakowski RS, Lewin SB, Miller MW (1989) Bromodeoxyuridine immunohistochemical determination of the lengths of the cell cycle and the DNA-synthetic phase for an anatomically defined population. J Neurocytol 18:311–318. CrossRef Medline

Palombella VJ, Mendelsohn J, VilcekJ (1988) Mitogenic action of tumor necrosis factor in human fibroblasts: interaction with epidermal growth factor and platelet-derived growth factor. J Cell Physiol 135:23–31. CrossRef Medline

Peukert K, Staller P, Schneider A, Carmichael G, Hänel F, Eilers M (1997) An alternative pathway for gene regulation by Myc. EMBO J 16:5672–5686. CrossRef Medline

Rothé B, Saliou JM, Quinternet M, Back R, Tiotiu D, Jacquemin C, Loegler C, Schlotter F, Peña V, Eckert K, Moréra S, Dorsselaer AV, Branlant C, Massenet S, Sanglier-Cianférani S, Manival X, Charpentier B (2014) Protein Hit1, a novel box C/D snoRNP assembly factor, controls cellular concentration of the scaffolding protein Rsa1 by direct interaction. Nucleic Acids Res 42:10731–10747. CrossRef Medline

Sanz-Moreno A, Fuhrmann D, Wolf E, von Eyss B, Eilers M, Elsässer HP (2014) Miz1 deficiency in the mammary gland causes a lactation defect by attenuated Stat5 expression and phosphorylation. PloS One 9:e89187. CrossRef Medline

Sanz-Moreno A, Fuhrmann D, Zankel A, Reingruber H, Kern L, Meijer D, Niemann A, Elsässer HP (2015) Late onset neuropathy with spontaneous clinical remission in mice lacking the POZ domain of the transcription factor Myc-interacting zinc finger protein 1 (Miz1) in Schwann cells. J Biol Chem 290:727–743. CrossRef Medline

Staller P, Peukert K, Kiermaier A, Seoane J, Lukas J, Karsunky H, Möröy T, Bartek J, Massagué J, Hänel F, Eilers M (2001) Repression of p15INK4b expression by Myc through association with Miz-1. Nat Cell Biol 3:392–399. CrossRef Medline

Stassart RM, Fledrich R, Velanac V, Brinkmann BG, Schwab MH, Meijer D, Sereda MW, Nave KA (2013) A role for Schwann cell-derived neuregulin-1 in remyelination. Nat Neurosci 16:48–54. CrossRef Medline

Stead MA, Wright SC (2014) Nac1 interacts with the POZ-domain transcription factor, Miz1. Biosci Rep 34:pii:e00110. CrossRef Medline

Stogios PJ, Downs GS, Jauhal JJ, Nandra SK, Privé GG (2005) Sequence and structural analysis of BTB domain proteins. Genome Biol 6:R82. CrossRef Medline

Svaren J, Meijer D (2008) The molecular machinery of myelin gene transcription in Schwann cells. Glia 56:1541–1551. CrossRef Medline

Wagner EJ, Carpenter PB (2012) Understanding the language of Lys36 methylation at histone H3. Nat Rev Mol Cell Biol 13:115–126. CrossRef Medline

Weider M, Küspert M, Bischof M, Vogl MR, Hornig J, Loy K, Kosian T, Müller J, Hillgärtner S, Tamm ER, Metzger D, Wegner M (2012) Chromatin-remodeling factor Brg1 is required for Schwann cell differentiation and myelination. Dev Cell 23:193–201. CrossRef Medline

Witkowski L, Foulkes WD (2015) In brief: picturing the complex world of chromatin remodelling families. J Pathol 237:403–406. CrossRef Medline

Wolf E, Gebhardt A, Kawauchi D, Walz S, von Eyss B, Wagner N, Renninger C, Krohne G, Asan E, Roussel MF, Eilers M (2013) Miz1 is required to maintain autophagic flux. Nat Commun 4:2535. CrossRef Medline

Zanazzi G, Einheber S, Westreich R, Hannocks MJ, Bedell-Hogan D, Marchionni MA, Salzer JL (2001) Glial growth factor/neuregulin inhibits Schwann cell myelination and induces demyelination. J Cell Biol 152:1289–1299. CrossRef Medline

Zhang T, Cooper S, Brockdorff N (2015) The interplay of histone modifications—writers that read. EMBO Rep 16:1467–1481. CrossRef Medline

Zhao Z, Sun C, Li F, Han J, Li X, Song Z (2015) Overexpression of histone demethylase JMJD5 promotes metastasis and indicates a poor prognosis in breast cancer. Int J Clin Exp Pathol 8:10325–10334. Medline

Zhu H, Hu S, Baker J (2014) JMJD5 regulates cell cycle and pluripotency in human embryonic stem cells. Stem Cells 32:2098–2110. CrossRef Medline

Zitouni S, Nabais C, Jana SC, Guerrero A, Bettencourt-Dias M (2014) Polo-like kinases: structural variations lead to multiple functions. Nat Rev Mol Cell Biol 15:433–452. CrossRef Medline